NASA Technical Memorandum 109131

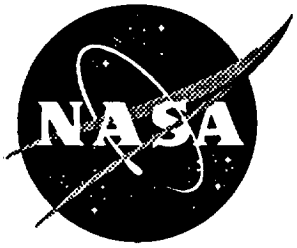

Stable Tearing Behavior of a Thin-Sheet Material with Multiple Cracks

D. S. Dawicke
Analytical Services and Materials, Inc., Hampton, Virginia

J. C. Newman, Jr.
Langley Research Center, Hampton, Virginia

M. A. Sutton and B. E. Amstutz
University of South Carolina, Columbia, South Carolina

July 1994

National Aeronautics and
Space Administration
Langley Research Center
Hampton, Virginia 23681-0001

STABLE TEARING BEHAVIOR OF A THIN-SHEET MATERIAL WITH MULTIPLE CRACKS

D. S. Dawicke, J. C. Newman, Jr., M. A. Sutton, and B. E. Amstutz

ABSTRACT

Fracture tests were conducted on 2.3mm thick, 305mm wide sheets of 2024-T3 aluminum alloy with from one to five collinear cracks. The cracks were introduced (crack history) into the specimens by three methods: saw cutting, fatigue precracking at a low stress range, and fatigue precracking at a high stress range. For the single crack tests, the initial crack history influenced the stress required for the onset of stable crack growth and the first 10mm of crack growth. The effect on failure stress was about 4% or less. For the multiple crack tests, the initial crack history was shown to cause differences of more than 20% in the link-up stress and 13% in failure stress. An elastic-plastic finite element analysis employing the CTOA fracture criterion was used to predict the fracture behavior of the single and multiple crack tests. The numerical predictions were within 7% of the observed link-up and failure stress in all the tests.

INTRODUCTION

Commercial jet transport aircraft are designed with economic fatigue design life goals. As the fleet ages and approaches its design life, the possibility for the development of fatigue cracking increases. Analysis tools are needed to assess the influence of fatigue cracks on structural integrity and to define inspection intervals. One of the objectives of the NASA Aircraft Structural Integrity Program [1] is to develop the methodology necessary to predict residual strength of cracked pressurized aircraft fuselage structures. The approach taken is to develop a local fracture criterion that can be used with shell-code finite element analyses. The fracture criterion should be able to predict large amounts of stable crack growth for multiple cracks under conditions of large-scale yielding in thin sheet materials.

The crack tip opening angle (CTOA) [2-6] fracture criterion has been experimentally verified to successfully predict residual strength in laboratory specimens [7-9]. Newman et al [10] have also applied the CTOA criteria to multiple-site damage (MSD) cracking scenarios, accurately predicting crack link-up and residual strength for 508mm wide sheets of clad 2024-T3 aluminum with 1 to 5 collinear cracks. That study indicated that, as postulated by Swift [11] and demonstrated experimentally by Maclin [12], the residual strength of a structure with a single long crack is significantly reduced

by the presence of smaller adjacent cracks. Furthermore, Newman et al [10] indicated that methods used to introduce cracks (fatigue precracking or saw cuts) can significantly influence the residual strength of multiple interacting cracks. The stress required for the onset of stable tearing was greater for saw cuts than for fatigue cracks. Increasing the fatigue precracking stress was also observed to increase the stress required for the onset of stable tearing [8]. These increases may have significant consequences on the link-up and failure of MSD cracking scenarios.

The objective of this study was to experimentally investigate the affect of crack history (including saw cuts) on the residual strength of multiple interacting cracks. Fracture tests were conducted on flat sheets test specimens containing from one to five cracks. The cracks were introduced into the specimens by three methods: saw cutting, fatigue precracking at a low stress range, and fatigue precracking at a high stress range. CTOA and strain field measurements were made on many of the tests. Predictions of the fracture behavior were made using an elastic-plastic finite element analysis and the critical CTOA fracture criterion.

EXPERIMENTAL PROCEDURE

Fracture tests were conducted on 2.3mm thick 2024-T3 aluminum alloy. The yield stress and ultimate strength of the material were 345 and 490 MPa, respectively. The specimens were 305mm wide and had from one to five nearly collinear cracks. Four additional tests were conducted on 76mm wide middle crack tension (M(T)) specimens. The cracks were introduced into the specimen by either fatigue precracking or by saw cuts. Measurements of CTOA were made using the digital image correlation (DIC) and optical microscope (OM) techniques. The strain field measurements were made using the DIC method.

Fracture Tests

All of the specimens were cracked in the L-T orientation (i.e., the load was applied in the longitudinal or rolling direction and the crack was in the transverse direction or perpendicular to the longitudinal direction). The cracks were introduced by fatigue precracking at a high stress range (HS), fatigue precracking at a low stress range (LS), or saw cutting (SC). The saw cuts were made with a jeweler's saw blade that made

a square-corner notch with roughly a 0.4mm slot height. The fatigue cracks were obtained by cycling notched specimens at a stress ratio of R=0.02 and at a stress range that would result in a stress intensity factor range of about 7 MPa $\sqrt{m}$ for the LS tests and about 35 MPa $\sqrt{m}$ for the HS tests. The multiple (3 and 5) crack specimens were fatigue precracked by first saw cutting notches at the intended locations of the smaller (MSD) cracks. The notch lengths were roughly 5mm less than the intended crack lengths. A stress range was calculated that resulted in the proper stress intensity factor range for the smaller cracks and the specimen fatigue precracked until the cracks reached the required length. Then, the longer crack was added by a saw cut, a new stress range calculated, and the specimen was again fatigue precracked until the long crack reached the required length. During the long crack fatigue precracking, the stress intensity factor of the smaller cracks was low enough that no noticeable crack growth was observed. Typical initial crack configurations are shown in Figure 1.

The specimens were fractured under displacement control. The rate of displacement was 3mm/sec. Anti-buckling guides were used in all but four tests. The anti-buckling guides consisted of two 12mm thick plates of 2024-T3 aluminum that sandwiched the specimen and were held in place by a series of bolts along the vertical edges. A layer of Teflon tape was put on the plates to reduce the friction between the plates and the specimen. The guides had a 10mm high and 250mm long slot in the center of the plate to view the cracks. During each test, measurements of some or all of the following parameters were made: load, crack length, surface CTOA, and surface strain fields.

Measurement Techniques

The critical CTOA during stable tearing was measured by direct observation of the surface using both the DIC and the OM techniques. The OM technique uses a video camera and a long focal length microscope to image the tearing crack. The CTOA is calculated directly from the angle made by points located on the upper surface, the crack tip and the lower surface [8, 9]. Similarly, the DIC technique uses a computer controlled video camera and lens system to digitize images of the specimen surface. To make measurements with the DIC technique, the specimen surface was coated with a high contrast random speckle pattern. A small region, or subset, is identified in a reference image and the relative displacement of that same subset in a subsequent image is calculated [8, 9, 13-17]. The CTOA measurement is based on displacements of subsets

located near the upper and lower crack surfaces and the crack tip [8, 9]. For both the DIC and OM techniques, the CTOA measurements were made within 0.5-1.5mm behind the crack tip.

The surface strain fields were calculated using the DIC technique. A displacement field grid was obtained by systematically measuring the displacements of overlapping subsets ahead of the crack tip. The displacement data was smoothed using a two-dimensional, optimal smoothing method [18]. The smoothing program computed the estimated surface strains ε_{yy}, ε_{xx}, and ε_{xy} at each displacement grid location. The strain field measurements were made in front of cracks or saw cuts in the 76mm wide specimens and in the ligaments between 2 cracks or 2 saw cuts in the 305mm wide specimens.

FINITE ELEMENT ANALYSIS

The elastic-plastic finite element code ZIP2D [19] was used to predict the stable tearing behavior in the fracture tests. The program uses 3-noded, constant strain triangular elements and a critical CTOA criterion to extend the crack. The elastic-plastic analysis employs the initial-stress concept [20] based on incremental flow theory and small strain assumptions. A multi-linear representation of the uniaxial stress-strain curve for 2024-T3, with the data given in Table 1, was used in the analysis with a von Mises yield criterion.

Finite Element Code and Meshes

The element size along the line of crack extension was d=0.48mm. Symmetry conditions required that only half of the specimen be modeled, with the axis of symmetry along the crack line. Normally, the nodes along the crack line and ahead of the crack tip are fixed, while those behind are free. This analysis uses springs along the crack line to change boundary conditions associated with crack extension. The spring stiffness is set equal to zero for nodes behind the crack tip and assigned an extremely large value for nodes ahead of the crack tip. Monotonic loading (under displacement control) was applied to the model. Crack growth by stable tearing was governed by the critical CTOA criterion. Reference 7 contains the details of the elastic-plastic finite element analysis used in this work.

Critical CTOA Criterion

The critical CTOA (ψ_c) criterion is equivalent to a critical CTOD (δ_c) value at a specified distance, d, behind the crack tip equal to one element length and is given by:

$$\psi_c = 2 \tan^{-1}\left(\delta_c/d\right) \quad (1)$$

The crack-tip node was released and the crack advanced to the next node whenever the CTOA equaled or exceeded a preset critical value (ψ_c) during incremental loading. This process was repeated until crack growth became unstable under load control or the crack reached a desired length under displacement control. The critical CTOA value (ψ_c) was determined experimentally from surface measurements made using both the OM and DIC techniques.

Crack History Simulation

The different crack histories (LS, HS, and SC) were simulated within the finite element analysis. The crack history associated with the low and high fatigue precracking was simulated by cyclic loading of the finite element model. The model was loaded to the appropriate stress level and the crack allowed to advance one element length, then the load returned to zero. The procedure was repeated for another cycle to allow residual stresses to develop ahead of the crack and plasticity deformed material left in the crack wake.

The saw cut was simulated by using the assumption that the saw cut must undergo a deformation, δ_i, at the tip before a crack would initiate. The saw cut tip node would be released once the tip displacement reached δ_i. The value δ_i was obtained by matching the crack growth in the single saw cut fracture tests. Additional information on determining δ_i for the saw cut simulation is given in Reference 10.

RESULTS AND DISCUSSION

Twenty nine fracture tests were conducted on the 305mm wide, 2.3mm thick sheets of 2024-T3 aluminum alloy. The tests are summarized in Table 2 and the initial crack configurations are given in Table 3. The critical CTOA was obtained from

experimental measurements made on a stably tearing crack. Four fracture tests were conducted on 76mm wide, 2.3mm middle crack tension specimens (M(T)) made of the same material. The M(T) tests are summarized in Table 4.

Single Crack Fracture Tests

Four different types of single crack fracture tests were conducted: low stress range fatigue precracking with anti-buckling guide plates (LS), low stress range fatigue precracking without anti-buckling guide plates (LS-NG), high stress range fatigue precracking (HS), and saw cuts (SC). In each test, the crack extension (Δa) was recorded as a function of applied stress. The failure stress was recorded for each test and is shown in Figure 2 as a function of the initial crack length. The LS and HS test had about the same failure stresses. The failure stresses of the SC and LS-NG tests were about 4% higher and about 13% lower, respectively than the failure stresses in the LS tests.

In each test, the amount of stable crack growth was measured as a function of applied stress, as shown in Figure 3 for the tests with the 127mm initial cracks. The LS-NG and LS tests were identical except for the use of anti-buckling guides in the LS test. The lack of anti-buckling guides decreased both the stress required for the initial crack growth and the failure stress. Compared to the LS test, the LS-NG test had a 6% lower stress at the onset of stable crack growth (indicated by the solid symbols) and a 16% lower failure stress. In the LS-NG tests, out-of-plane displacements were measured at the center of the crack (6mm above the crack plane), as shown in Figure 4. The out-of-plane displacements initially increased linearly with applied stress, but above a stress of 80MPa the displacements increased dramatically, indicating the start of local crack buckling.

The HS and LS tests differed only in the stress range used for the initial fatigue precracking. The high stress range fatigue precracking increased the plastic deformation ahead of the crack and in the crack wake, increasing the stress required to initiate stable crack growth by 16% compared to the LS test. After about 10mm of stable crack growth, the influence of the initial crack history was lost and the behavior of the LS and HS tests were identical, as shown in Figure 3.

The stress required to initiate stable crack growth from a saw cut was about 47% higher than that of the LS test, but the failure stress was only increased by about 4%. The SC test required about 20mm of crack growth before the effect of the saw cut had

diminished and the crack growth behavior approached that of the LS and HS tests, as shown in Figure 3.

Multiple Crack Fracture Tests

Three different techniques (LS, HS, and SC) were used to introduce cracks for the multiple crack fracture tests. Three patterns of multiple cracks were examined (Figure 1): two long cracks with a small ligament between them, a long centered crack with a single small crack in front of both crack tips (both small and large ligaments were considered), and a long centered crack with two small collinear cracks in front of both crack tips.

In the tests with three collinear cracks (with small ligaments between cracks), the link-up behavior of all three tests (LS, HS, and SC) was different, as shown in Figure 5. For the LS test, link-up occurred at 136 MPa and the highest stress occurred at a second loading peak, well after link-up. Link-up in the HS test occurred at a stress 7% higher than the stress in the LS test, but after link-up the two tests were nearly identical. The behavior of the SC test was noticeably different. Link-up occurred at 166 MPa, 22% greater than in the LS test, and this was the maximum stress in the test. A second peak stress was observed, but this was less than the link-up stress. The crack growth behavior of the SC test agreed with the LS and HS tests after about 25mm of crack extension. The actual difference in maximum stresses after link-up for the three tests was only about 5%, but the stable crack growth behavior of the three tests was considerably different.

Only LS and SC tests were conducted for the configuration of three collinear cracks with large ligaments between cracks, as shown in Figure 6. The onset of crack growth began at a stress of 187 MPa in the LS test and at a stress of 247 MPa in the SC test. Link-up was the critical event (maximum stress) in both tests, with the stress at failure in the SC test about 4% higher than the stress at failure in the LS test.

In the tests with five collinear cracks, the LS and HS link-up behavior was nearly identical, as shown in Figure 7. In the SC tests, the onset of crack growth occurred at stress level greater that the stress required for failure in the LS and HS tests. Link-up was the critical event in all three tests, with the link-up in the SC tests at a stress 13% higher than the stress in the LS and HS tests.

Strain Fields

The DIC method was used to measure the strain field in the ligament between two collinear cracks and between two collinear saw cuts. The fatigue cracks and saw cuts were about 50mm long and both large (15mm) and small (5mm) ligaments were examined. The cracks were fatigue precracked at a low stress level (LS) and the saw cuts (SC) were produced in the same manner as discussed earlier. For the small ligament tests, link-up occurred at 91 MPa and 126 MPa for the fatigue cracks and saw cuts, respectively. The failure stress was 209 MPa and 223 MPa for the fatigue cracks and saw cuts, respectively. For the large ligament tests, link-up occurred at 149 MPa and 181 MPa for the fatigue cracks and saw cuts, respectively. The failure stress was 195 MPa and 205 MPa for the fatigue cracks and saw cuts, respectively. Four ε_{yy} strain fields were generated for the tests with small ligaments: at 74%, 84%, 92%, and 94% of the link-up stress for the LS test and 53%, 86%, 91% and 99% of the link-up stress for the SC test, as shown in Figures 8-11, respectively.

The LS strain field at 74% of the link-up stress (Figure 8a) and the SC strain field at 53% of the link-up stress (Figure 8b) were at the same stress level (S=67 MPa). The strain in the direction of loading (ε_{yy}) throughout the LS ligament are clearly greater than those of the SC ligament and the strains in the LS ligament are above a yield strain of 0.007. After increasing the applied stress to 84% and 86% of the link-up stresses for the LS (Figure 9a) and SC (Figure 9b) tests, respectively, the ε_{yy} strain in the ligament between the two cracks exceeds 0.02. The strain contour lines depict the twin lobes of elevated strain near the crack tip and saw cut. The lobes for the saw cut are more spread out, while those in front of the crack tip are more concentrated and have higher strains. In the center of the ligament, the strains for both the LS and SC case are about the same. The LS strain fields at 92% and 94% of the link-up stress (Figures 10a and 11a) and the SC strain fields at 91% and 99% of the link-up stress (Figures 10b and 11b) continue to exhibit this trend. However, by 92% of the link-up stress, the crack has begun to grow. Crack growth from the saw cut does not begin until the link-up stress.

LS and SC fracture tests were conducted on the 76mm wide M(T) specimens. Crack growth began at a lower load in the LS tests than in the SC tests and the failure stress of the SC tests (248 MPa) were about 5% higher than the LS tests (237 MPa). The DIC method was used to measure the ε_{yy} strains ahead of the cracks and saw cuts. The ε_{yy} strains were measured along a line, perpendicular to the direction of loading, starting

at the region of maximum strain for both the crack tip and saw cut. Figure 12 contains the LS and SC ε_{yy} strains against the distance from the crack or saw cut for applied stress level of 230 MPa. As indicated by the strain field plots, for the same applies stress level the ε_{yy} strains ahead of the crack tip are consistently greater than those from the saw cut. This effect is highly localized because the ε_{yy} strains at distances greater than 1mm ahead of the crack or saw cut are nearly identical.

CTOA Measurements

The measured critical CTOA values as a function of crack extension for the tests with low stress range (LS) fatigue precracking are shown in Figure 13. Also shown in Figure 13 is the scatter band for the 76mm wide middle crack tension, M(T), tests conducted under LS conditions on the same material [8,9]. The measured CTOA values fall within the scatter band and have an average value of about 6° in the steady-state region beyond one thickness (2.3mm) of crack extension.

The measured critical CTOA values for the tests with high stress range (HS) fatigue precracking and with saw cuts (SC) are shown in Figure 14. Also shown in Figure 14 is the scatter band from the 76mm wide middle crack tension, M(T), tests conducted under HS conditions on the same material [8,9]. Again, the measured CTOA values fall within the scatter band and have an average value of about 6° in the steady-state region beyond about 2mm of crack extension.

Finite Element Predictions

The fracture experiments were predicted using the elastic-plastic finite element code ZIP2D, the stress-strain relationship given in Table 1, and the experimentally measured CTOA value of 6°. The critical displacement, δ_i, used to delay crack growth from the saw cuts, was determined by choosing a value that would best match the behavior of the three SC tests. The finite element analysis was terminated after all link-ups had occurred and the stress dropped for 20 increments of crack extension.

All of the predictions of stress at link-up and failure stress were within 5% of the values obtained from the experiments. The stress against crack extension results from the single crack LS tests and predictions are shown in Figure 15. Initially, the finite-element analysis overpredicted the amount of crack growth for a given applied stress. However,

severe tunneling has been observed in previous tests during this initial phase of stable tearing [8,9], resulting in more crack extension in the interior than measured on the surface. After about 4mm of stable crack growth, the predictions closely matched the experimental measurements for all three initial crack lengths.

The stress against crack extension results from the single crack HS tests and predictions are shown in Figure 16. Once again, the analysis overpredicted the initial amount of crack growth, but after about 4mm of stable crack growth, the predictions closely matched the experimental measurements for all three initial crack lengths. The simulated high fatigue stress range precracking caused the stress level required to initiate crack growth to be about 15% higher than required in the LS simulation. However, the failure stresses were not affected by the HS fatigue precracking.

The stress against crack extension results from the single crack SC tests and simulations are shown in Figure 17. These simulations were obtained by choosing a δ_i, value that would result in the best match to the stress against crack extension behavior. The chosen value was $\delta_i = 0.076$mm and this value was used in all subsequent SC predictions. The simulated saw cut behavior caused the stress level required to grow the crack to be about 50% higher than required in the LS simulation.

Predictions were made for the multiple crack fracture tests, the 3- and 5-crack configurations had a single long central crack and smaller collinear cracks, the 2-crack configurations had two roughly equal cracks with a ligament at the center of the specimen. The stress against crack extension results and predictions for the 3-crack (with small ligaments between cracks) fracture tests are shown in Figure 18. The predictions for all three crack histories (LS, HS, and SC) were in good agreement with the experimental measurements. Once again, the predicted initial crack growth was greater than observed experimentally, but the link-up and maximum stresses were within 2% of the experimental measurements. The stress against crack extension results and the predictions for the 3-crack (with large ligaments between cracks) fracture tests are shown in Figure 19. The predictions were in good agreement with the experimental results with the predicted link-up stresses (link-up occurred at maximum stress) were within 3% of the experimental measurements.

The stress against crack extension results and predictions for the 5-crack fracture tests are shown in Figure 20. The predictions for the LS and HS tests were in good

agreement with the experimental measurements, but the SC predictions for stress at link-up (link-up occurred at the maximum stress) were about 5% greater than measured in the experiments.

The stress against crack extension predictions and experimentally measured link-up and failure stresses (crack growth was not monitored in these tests) for the 2-crack fracture tests are shown in Figures 21 and 22 for the small and large ligament configurations, respectively. The predictions for the LS and SC tests were in good agreement with the experiments for both configurations. For the small ligament (5mm) configuration, the predicted link-up stresses were within 7% and the predicted failure stresses were within 5% of the experimental measurements. For the large ligament (15mm) configuration, the predicted link-up and failure stresses were within 6% of the experimental measurements.

CONCLUDING REMARKS

A combination of experimental and analytical methods has demonstrated that the stable crack growth behavior and residual strength of thin sheet structures with multiple collinear cracks, is influenced by the crack history and that this behavior can be accurately predicted. In particular, this research has shown that:

(1) The initial crack history (saw cut, high stress level fatigue precracking, low stress level fatigue precracking) has a strong effect on the initial portion of stable crack growth.

   (a) For a single crack, the influence of initial history (fatigue precracking stress level and saw cuts) is lost after about 10mm of crack growth. The effect on residual strength is about 4% or less.

   (b) For multiple collinear cracks, the initial history (fatigue precracking stress level and saw cuts) was shown to cause differences of more than 20% in link-up stress and 13% in failure stress.

(2) Saw cuts resulted in higher (unconservative) link-up and failure stresses than equivalent fatigue cracks. The behavior of saw cuts and cracks appears to be directly linked to experimentally observed differences in the local crack tip strain fields; the crack tip strains are highly concentrated, being much higher than the saw cut strains within 0.60mm of the tip (this corresponds to the large deformation region or fracture process zone).

(3) The ZIP2D plane stress finite element model, coupled with the experimentally measured critical CTOA = 6°, accurately predict the behavior for single crack and multiple collinear crack configurations.

(4) Accurate prediction of saw cut specimens requires both an initiation parameter, δ_i, as well as a critical CTOA.

(5) Unrestrained crack buckling can reduce the residual strength significantly.

REFERENCES

1. Harris, C. E., "NASA Aircraft Structural Integrity Program", NASA TM 102637, April 1990.

2 Anderson, H., "Finite Element Representation of Stable Crack Growth," Journal of Mechanics and Physics of Solids, Vol. 21, 1973, pp. 337-356.

3. de Koning, A. U., "A Contribution to the Analysis of Quasi Static Crack Growth in Steel Materials," in Fracture 1977, Proceedings of the 4th International Conference on Fracture, Vol. 3, pp. 25-31.

4. Wells, A. A., "Unstable Crack Propagation in Metals: Cleavage and Fast Fracture," in Proceedings of the Cranfield Crack Propagation Symposium, Vol. 1, 1961, pp. 210-230.

5. Wells, A. A., "Application of Fracture Mechanics at and Beyond General Yielding," British Welding Journal, Vol. 11, 1961, pp. 563-570.

6. Wells, A. A., "Notched Bar Tests, Fracture Mechanics and Brittle Strengths of Welded Structures," British Welding Journal, Vol. 12, 1963, pp. 2-13.

7. Newman, J. C., Jr., Dawicke, D. S., and Bigelow, C. A., "Finite-Element Analysis and Measurement of CTOA During Stable Tearing in a Thin-Sheet Aluminum Alloy," Proceedings from the International Workshop on Structural Integrity of Aging Airplanes, April 1992, pp. 167-186.

8. Dawicke, D. S. and Sutton, M. A., "Crack-Tip-Opening Angle Measurements and Crack Tunneling Under Stable Tearing in Thin Sheet 2024-T3 Aluminum Alloy", NASA-CR-191523, September 1993, also submitted to Experimental Mechanics.

9. Dawicke, D. S., Sutton, M. A., Newman, J. C., Jr., and Bigelow, C. A., "Measurement and analysis of Critical CTOA for an Aluminum Alloy Sheet", NASA-TM-109024, September 1993, also submitted to Fracture Mechanics: Twenty-Fifth National Symposium, ASTM STP 1220.

10. Newman, J. C., Jr., Dawicke, D. S., Sutton, M. A., and Bigelow, C. A., "A Fracture Criterion for Widespread Cracking in Thin-Sheet Aluminum Alloys", 17th International Committee on Aeronautical Fatigue, June 1993.

11. Swift, T., "Damage Tolerance in Pressurized Fuselages", 14th International Conference on Aeronautical Fatigue, 1987.

12. Maclin, J., NASA CP-3160, Washington, DC, 1992, pp. 67-75.

13. Sutton, M. A., Bruck, H. A., Chae, T. L., and Turner, J. L., "Experimental Investigations of Three-Dimensional Effects Near a Crack Tip Using Computer Vision," International Journal of Fracture, Vol. 53, 1991, pp. 201-228.

14. Sutton, M. A., Bruck, H. A., and McNeill, S. R., "Determination of Deformations Using Digital Correlation with the Newton Raphson Method for Partial Differential Correction," Experimental Mechanics, Vol. 29 (3), 1989, pp. 261-267.

15. Sutton, M. A., Turner, J. L., Chae, T. L., and Bruck, H. A., "Development of a Computer Vision Methodology for the Analysis of Surface Deformation in Magnified Image," ASTM STP 1094, MICOM 90. 1990, pp. 109-132.

16. Sutton, M. A., Turner, J. L., Bruck, H. A., and Chae, T. L., "Full-Field Representation of the Discretely Sampled Surface Deformation for Displacement and Strain Analysis," Experimental Mechanics, Vol. 31 (2), 1991, pp. 168-177.

17. Sutton, M. A. and McNeill, S. R., "The Effects of Subpixel Image Restoration on Digital Correlation Error Estimates," Optical Engineering, Vol. 27 (3), 1988, pp. 163-175.

18. Dohrmann, C. R. and Bushy, H. R., "Spline Function Smoothing and Differentiation of Noisy Data on a Rectangular Grid," Proceedings of the VI International Conference on Experimental Mechanics, pp. 843-849, 1988.

19. Newman, J. C., Jr., "Finite-Element Analysis of Fatigue Crack Propagation--Including the Effects of Crack Closure," Ph.D. Thesis, VPI & State University, Blacksburg, VA, May 1974.

20. Zienkiewicz, O. C., Valliappan, S., and King, I. P., "Elasto-Plastic Solutions of Engineering Problems, Initial Stress, Finite Element Approach," International Journal of Numerical Methods in Engineering, Vol. 1, 1969, pp. 75-100.

21. Hom, C. L. and McMeeking, R. M., "Large Crack Tip Opening in thin, elastic-plastic sheets", International Journal of Fracture, Vol 45, 1990, pp 103-122.

22. McMeeking, R. M., "Finite Deformation Analysis of Crack Tip Opening in Elastic-Plastic Materials and Implications for Fracture", Journal of Mechanics and Physics of Solids, Vol 35, 1977, pp 357-381.

23. McMeeking, R. M., "Recent Advances in Fracture Mechanics", Fracture Mechanics: Microstructure and Mechanisms, ASM Intl, 1987, pp. 1-30.

TABLE 1 Multi-linear representation of the uniaxial stress-strain curve for 2024-T3.

σ (MPa)	ε	
345	0.00483	E = 71,400 MPa ν = 0.3
390	0.015	
430	0.04	
470	0.1	
490	0.16	
490	0.2	

TABLE 2 Test summary for the 304.8mm wide fracture tests

Test ID	Number of Cracks	Precrack Stress Range		Initial Total Crack Length (mm)	Fracture Stress (MPa)	Type	Ligament Link-Up Stress (MPa)			
		Small Cracks (MPa)	Long Crack (MPa)				L1 (MPa)	L2 (MPa)	L3 (MPa)	L4 (MPa)
MT-12-01	1	--	17.2	101.5	195.0	LS-NG[1]	--	--	--	--
MT-12-02	1	--	17.2	101.4	215.5	LS	--	--	--	--
MT-12-04	5	110.3	22.4	133.5	161.4	LS	161.4	161.4	161.4	161.4
MT-12-05	5	--	--	131.8	182.1	SC	182.1	182.1	182.1	182.1
MT-12-06	1	--	--	101.7	220.6	SC	--	--	--	--
MT-12-07	3	76.6	19.2	126.6	158.3	LS	136.1	135.8	--	--
MT-12-08	3	--	--	125.7	166.3	SC	166.3	164.4	--	--
MT-12-09	3	63.8	31.9	76.6	258.6	LS	258.6	258.6	--	--
MT-12-10	3	--	--	75.8	269.5	SC	269.5	269.5	--	--
MT-12-11	1	--	86.2	101.5	219.5	HS	--	--	--	--
MT-12-12	3	255.4	83.0	126.2	160.1	HS	146.3	145.7	--	--
MT-12-13	5	255.4	83.0	152.6	136.3	HS	136.3	136.3	126.9	126.9
MT-12-14	5	255.4	83.0	134.4	161.2	HS	161.2	161.2	161.2	161.2
MT-12-15	1	--	16.0	126.1	190.8	LS	--	--	--	--
MT-12-16	1	--	16.0	133.4	181.9	LS	--	--	--	--
MT-12-17	2	--	21.1	98.5	208.7	LS	91.0	--	--	--
MT-12-18	3	76.6	19.2	126.4	171.2	LS	171.2	171.2	--	--
MT-12-19	2	--	21.1	100.0	194.5	LS	149.1	--	--	--
MT-12-20	1	--	17.2	101.5	196.8	LS-NG	--	--	--	--
MT-12-21	1	--	16.0	127.0	161.7	LS-NG	--	--	--	--
MT-12-22	1	--	13.3	152.4	136.2	LS-NG	--	--	--	--
MT-12-23	2	--	--	97.7	204.7	SC	181.4	--	--	--
MT-12-24	2	--	--	95.9	223.4	SC	126.1	--	--	--
MT-12-25	1	--	16.0	127.0	186.1	LS	--	--	--	--
MT-12-26	1	--	13.3	152.4	160.9	LS	--	--	--	--
MT-12-27	1	--	--	150.5	169.2	SC	--	--	--	--
MT-12-28	1	--	--	124.8	196.8	SC	--	--	--	--
MT-12-29	1	--	63.8	152.4	158.5	HS	--	--	--	--
MT-12-30	1	--	76.6	127.1	187.3	HS	--	--	--	--

Note: [1] LS = low stress range precracking, NG =no anti-buckling guides, HS = high stress range precracking, and SC = saw cut

TABLE 3 Initial Crack Configurations for the 305mm Wide Fracture Tests

Test ID	$2a_1$	L_1	$2a_2$	L_2	$2a_3$	L_3	$2a_4$	L_4	$2a_5$
MT-12-01	101.5	--	--	--	--	--	--	--	--
MT-12-02	101.4	--	--	--	--	--	--	--	--
MT-12-04	7.4	17.3	8.0	18.3	101.5	18.8	8.4	17.0	8.1
MT-12-05	7.4	16.5	9.1	19.9	100.3	17.8	8.0	18.0	7.0
MT-12-06	101.7	--	--	--	--	--	--	--	--
MT-12-07	13.8	12.3	101.5	14.1	12.3	--	--	--	--
MT-12-08	13.6	12.5	100.7	14.9	11.3	--	--	--	--
MT-12-09	11.6	51.1	50.7	49.9	14.4	--	--	--	--
MT-12-10	11.7	50.3	50.3	49.9	13.8	--	--	--	--
MT-12-11	101.5	--	--	--	--	--	--	--	--
MT-12-12	14.8	12.6	101.4	14.5	9.9	--	--	--	--
MT-12-13	14.2	9.7	16.7	13.7	101.3	18.9	10.9	15.7	9.4
MT-12-14	9.4	15.2	9.7	15.1	101.5	15.2	6.6	19.0	6.8
MT-12-15	126.1	--	--	--	--	--	--	--	--
MT-12-16	133.4	--	--	--	--	--	--	--	--
MT-12-17	50.6	5.1	47.9	--	--	--	--	--	--
MT-12-18	12.8	24.2	101.4	26.7	12.2	--	--	--	--
MT-12-19	47.3	15.2	52.6	--	--	--	--	--	--
MT-12-20	101.6	--	--	--	--	--	--	--	--
MT-12-21	127.0	--	--	--	--	--	--	--	--
MT-12-22	152.4	--	--	--	--	--	--	--	--
MT-12-23	51.5	16.0	46.2	--	--	--	--	--	--
MT-12-24	48.3	5.2	47.6	--	--	--	--	--	--
MT-12-25	127.0	--	--	--	--	--	--	--	--
MT-12-26	152.4	--	--	--	--	--	--	--	--
MT-12-27	150.5	--	--	--	--	--	--	--	--
MT-12-28	124.8	--	--	--	--	--	--	--	--
MT-12-29	152.4	--	--	--	--	--	--	--	--
MT-12-30	127.1	--	--	--	--	--	--	--	--

TABLE 4 Test Summary for the 76mm Wide Single Crack Fracture Tests

Test ID	Precrack Stress Range (MPa)	Initial Crack Length (mm)	Fracture Stress (MPa)	Test Type
MT-03-123	--	25.3	249.5	SC
MT-03-124	--	25.3	245.7	SC
MT-03-125	34.5	25.4	238.0	LS
MT-03-126	34.5	25.4	235.7	LS

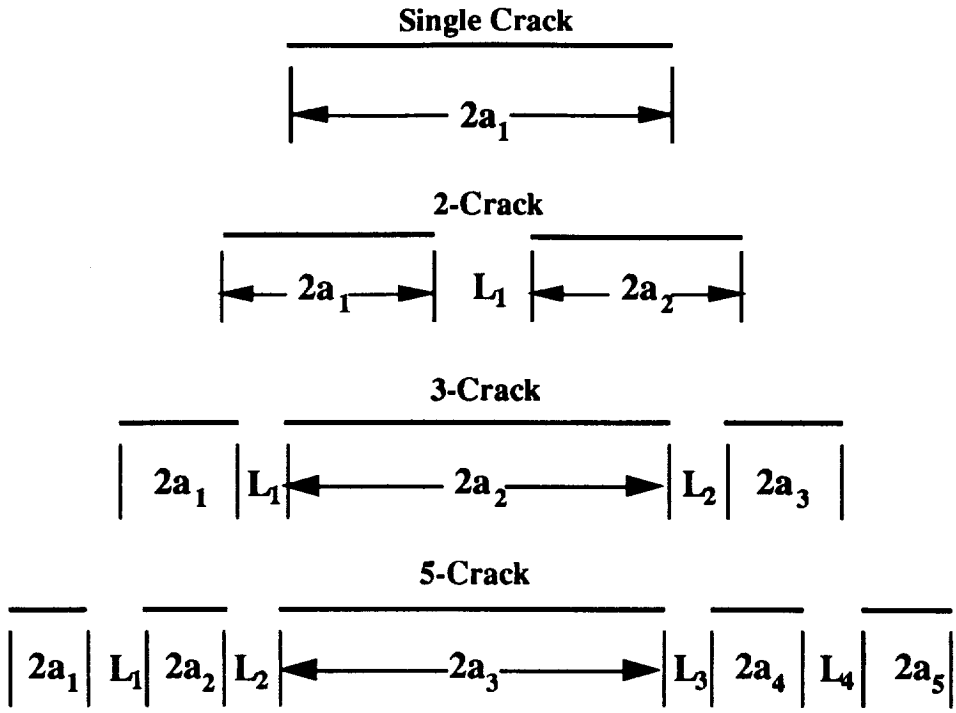

Figure 1. Schematic of crack configurations for fracture tests.

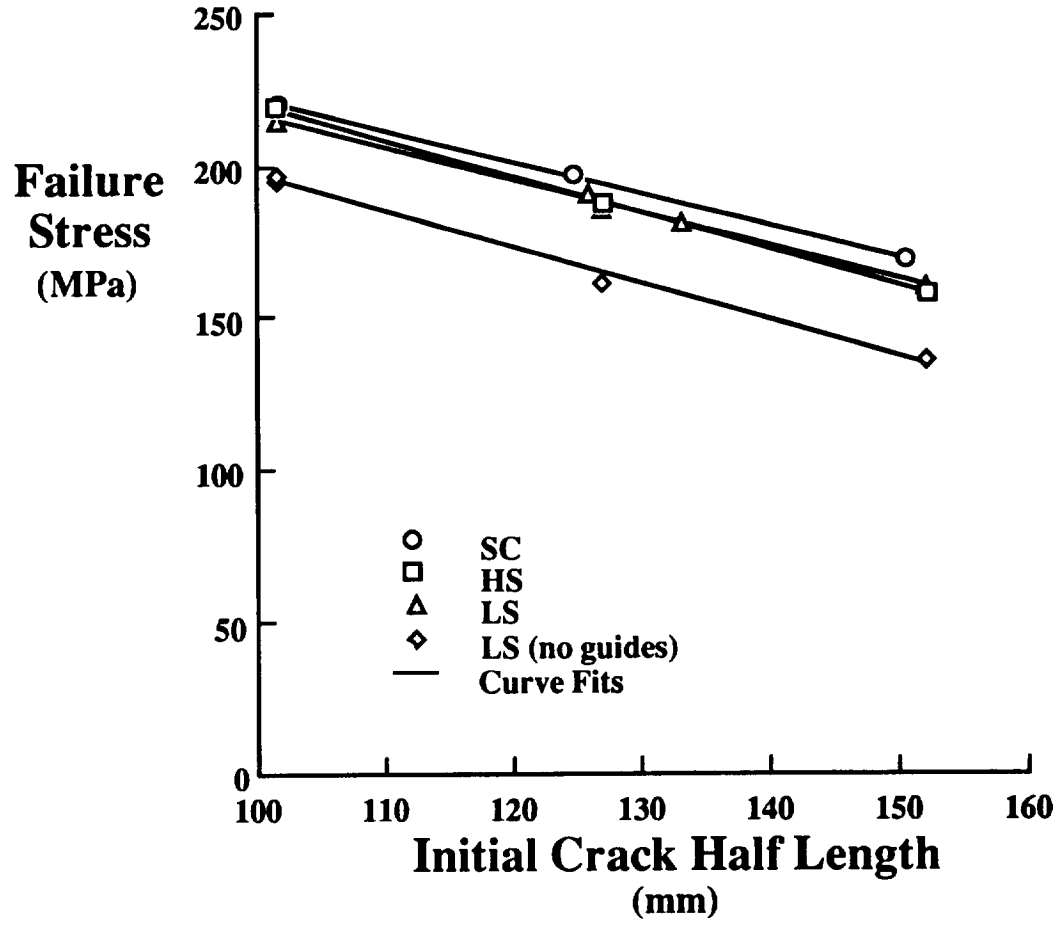

Figure 2 Maximum fracture stress as a function of initial crack length for the single crack fracture tests.

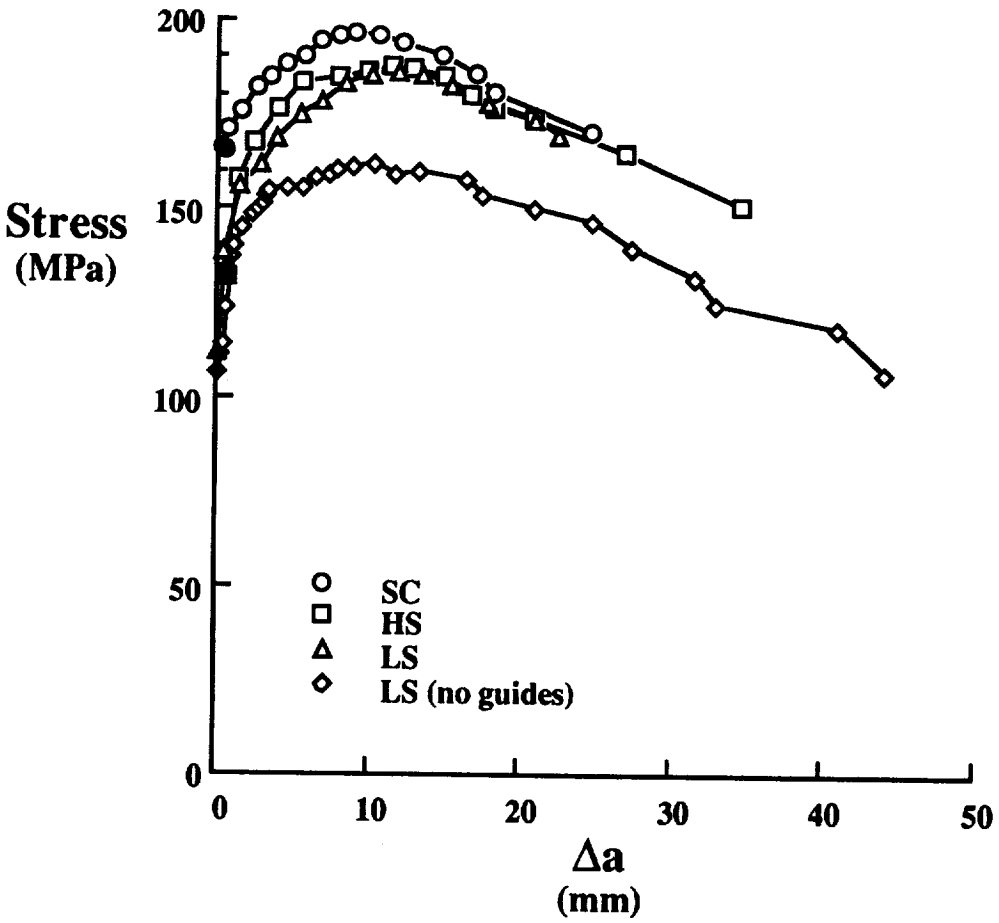

Figure 3 Stress against crack growth behavior for the single 127mm cracks (solid symbols indicate the onset of crack growth).

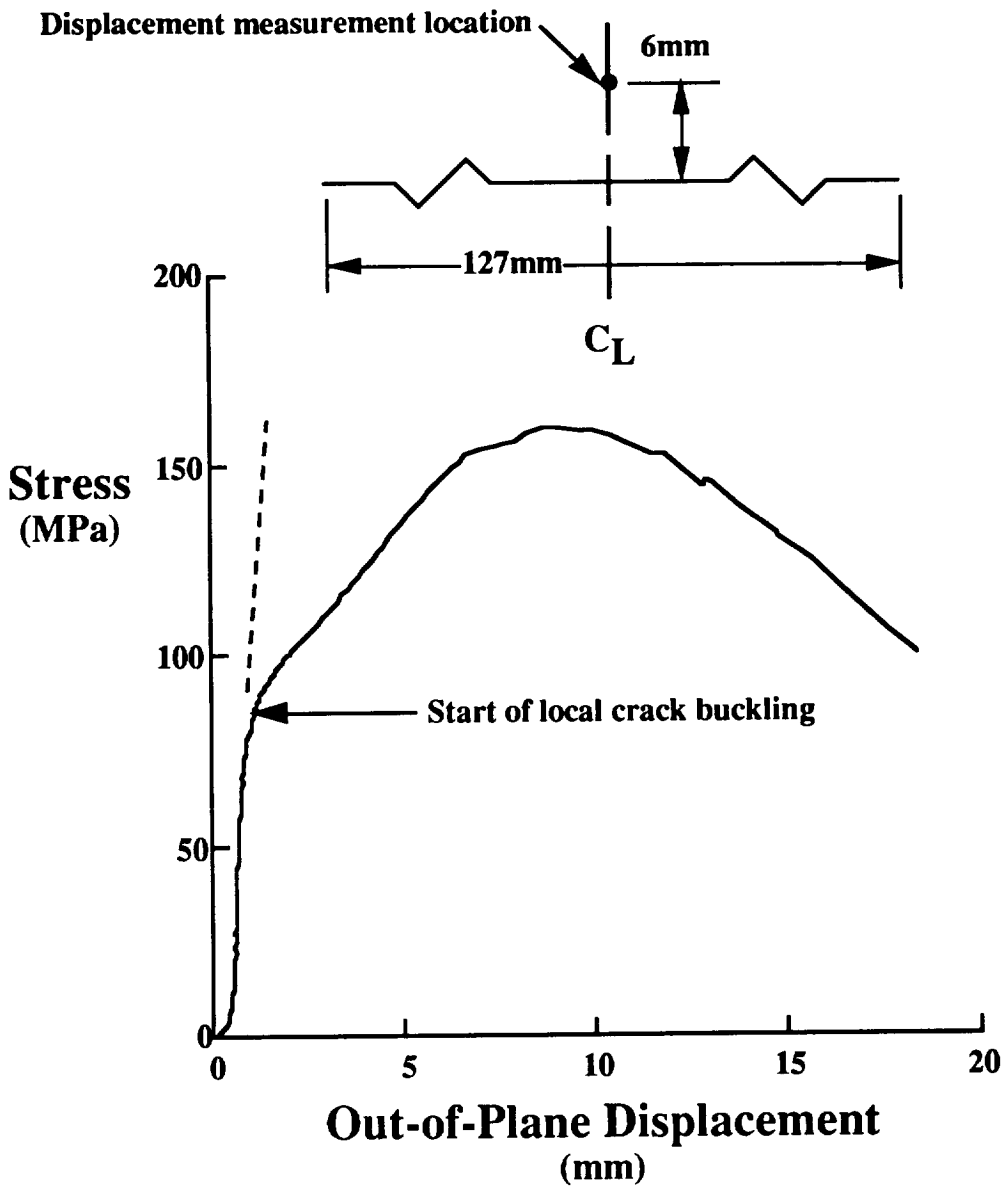

Figure 4 Crack plane out-of-plane displacement measurements for a 127mm initial single center crack without anti-buckling guides.

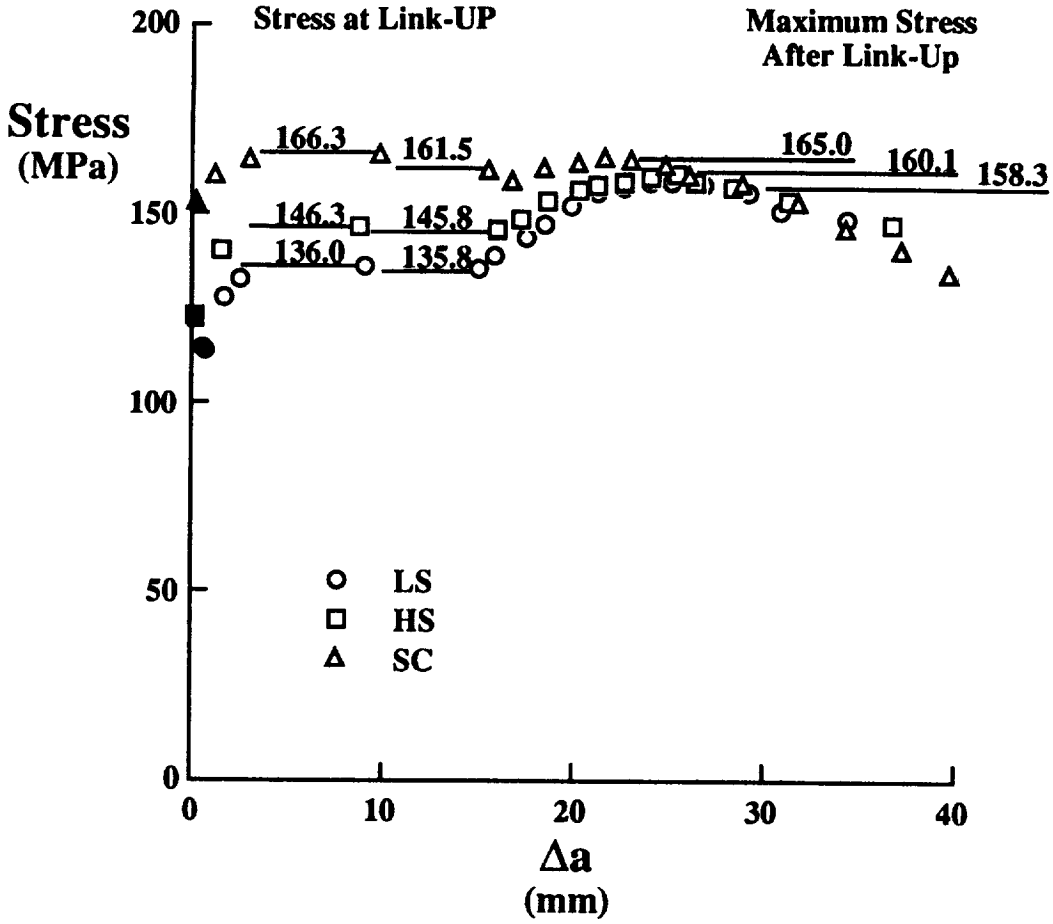

Figure 5 Applied stress against stable crack extension for the 3-crack fracture tests with small ligaments between cracks (solid symbols indicate the onset of crack growth).

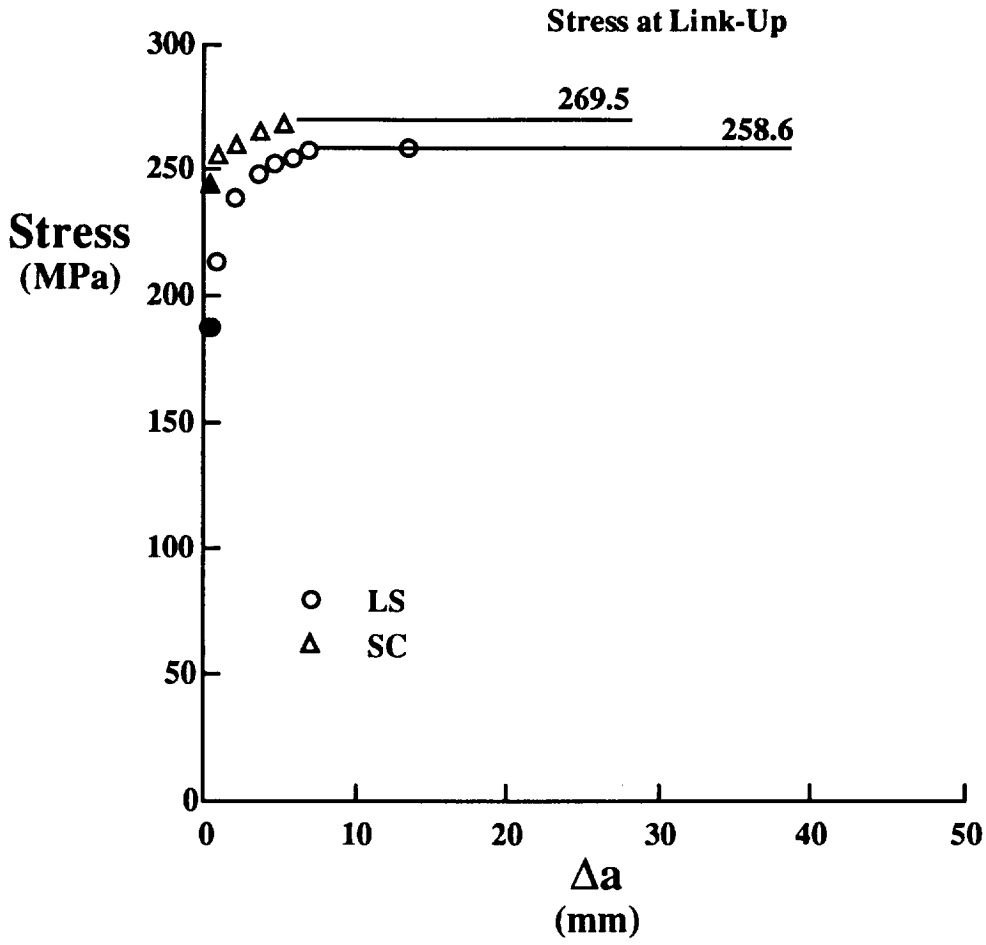

Figure 6 Applied stress against stable crack extension for the 3-crack fracture tests with large ligaments between cracks (solid symbols indicate the onset of crack growth).

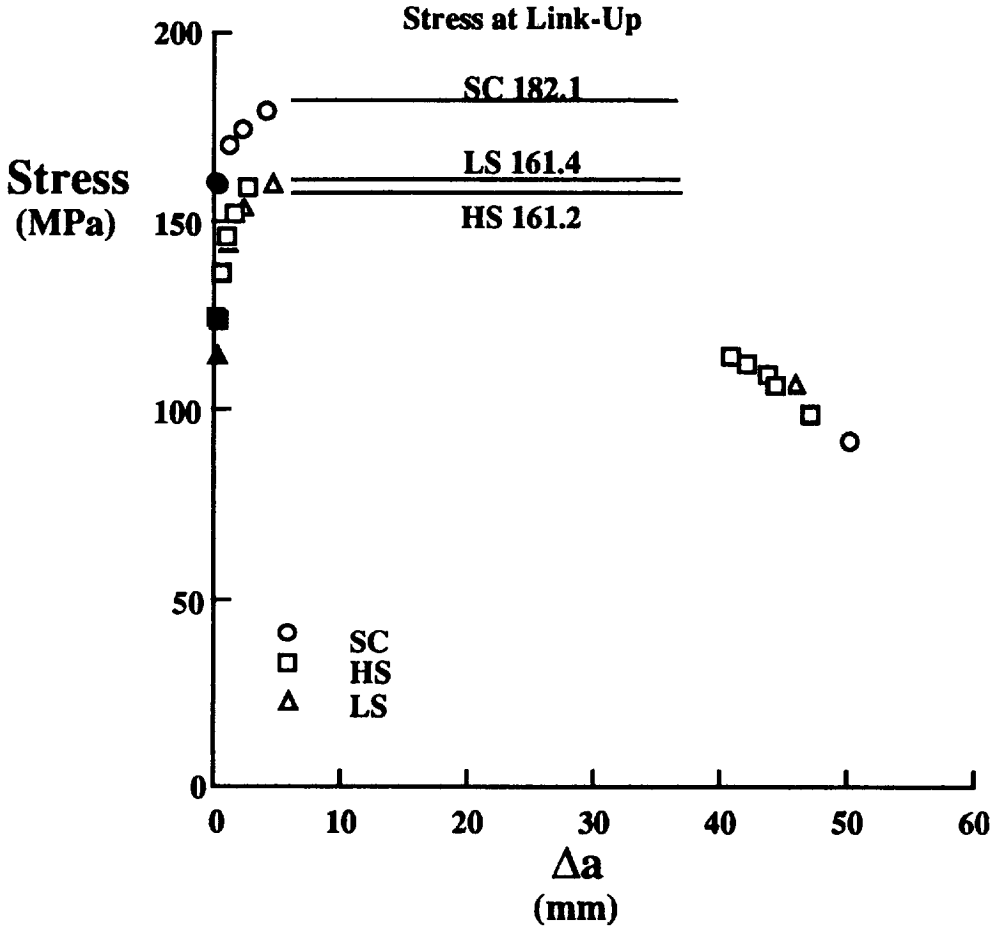

Figure 7 Applied stress against stable crack extension for the 5-crack fracture tests (solid symbols indicate the onset of crack growth).

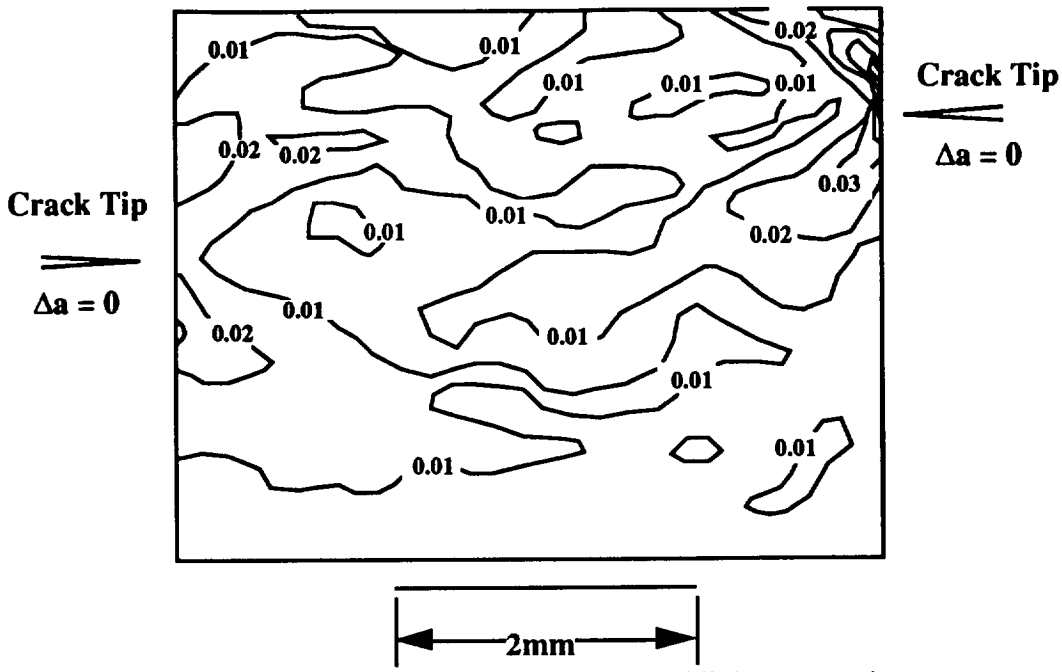

a. LS fracture tests (S=67 MPa, 74% of link-up stress)

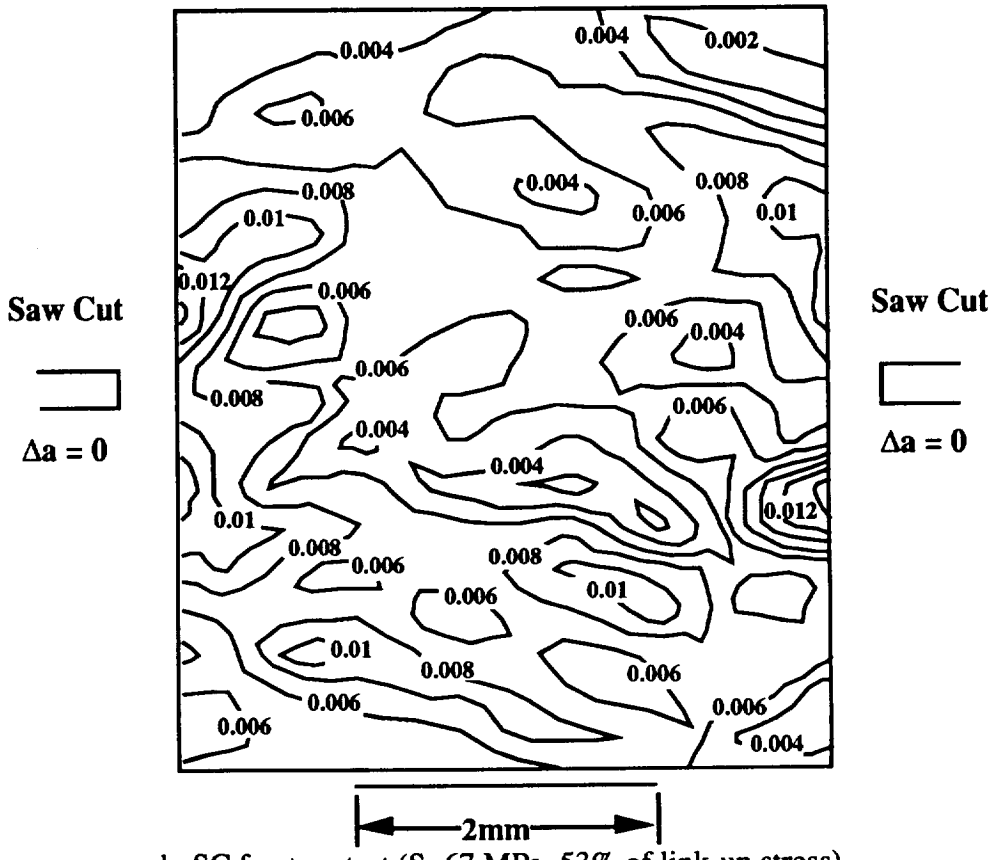

b. SC fracture test (S=67 MPa, 53% of link-up stress)

Figure 8 ε_{yy} strain fields for the ligament between two cracks 5mm apart.

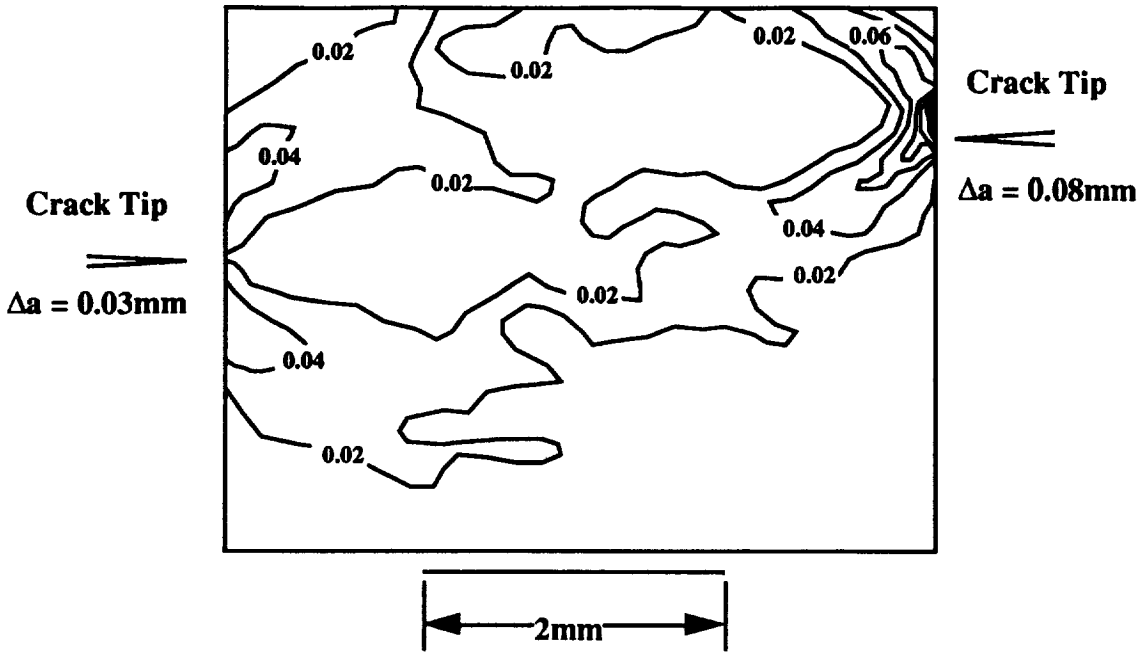

a. LS fracture tests (S=77 MPa, 84% of link-up stress)

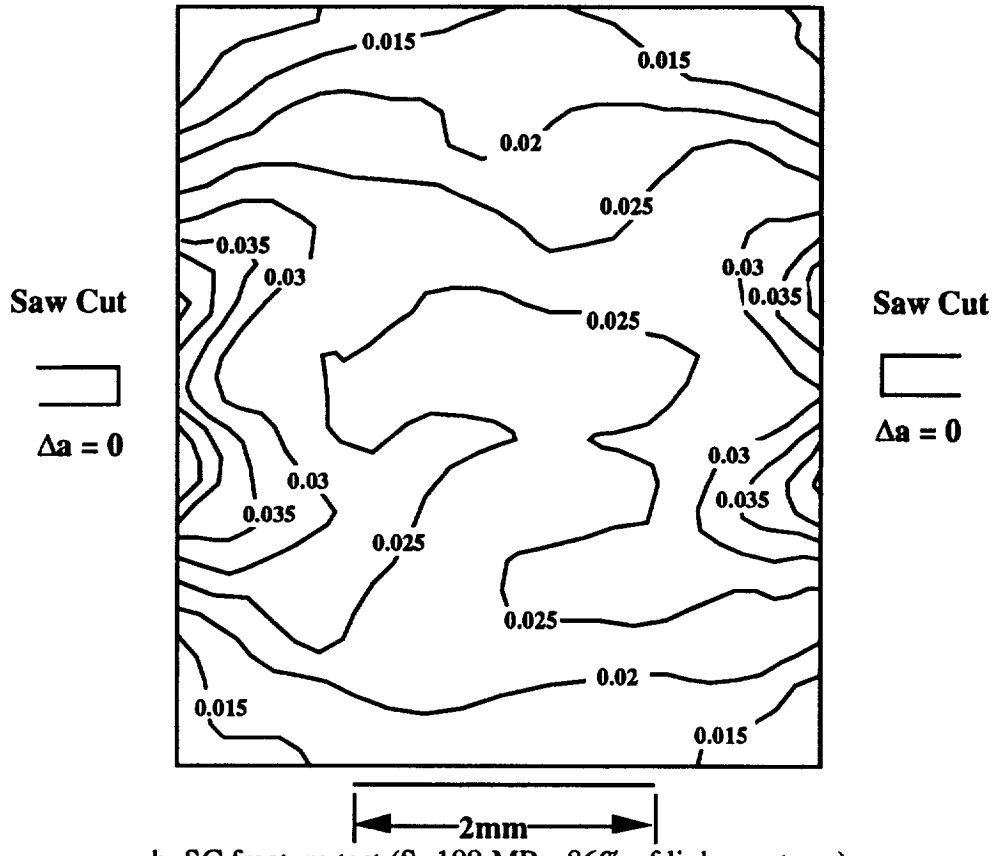

b. SC fracture test (S=109 MPa, 86% of link-up stress)

Figure 9 ε_{yy} strain fields for the ligament between two cracks 5mm apart.

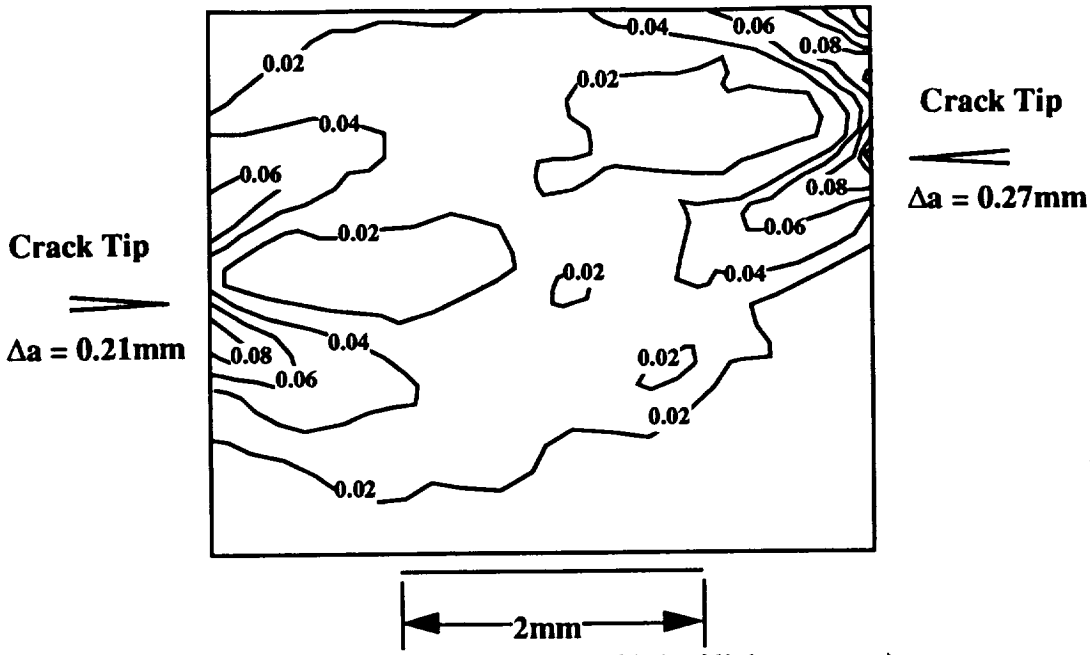

a. LS fracture tests (S=84 MPa, 92% of link-up stress)

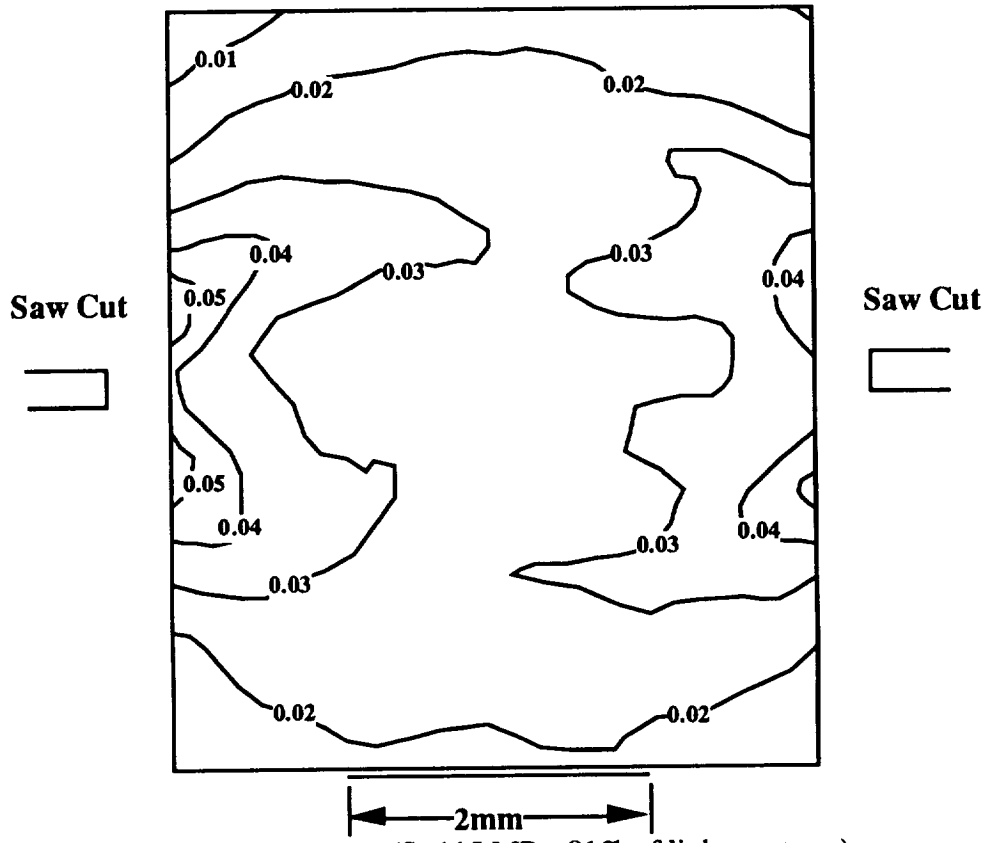

b. SC fracture test (S=115 MPa, 91% of link-up stress)

Figure 10 ε_{yy} strain fields for the ligament between two cracks 5.1mm apart.

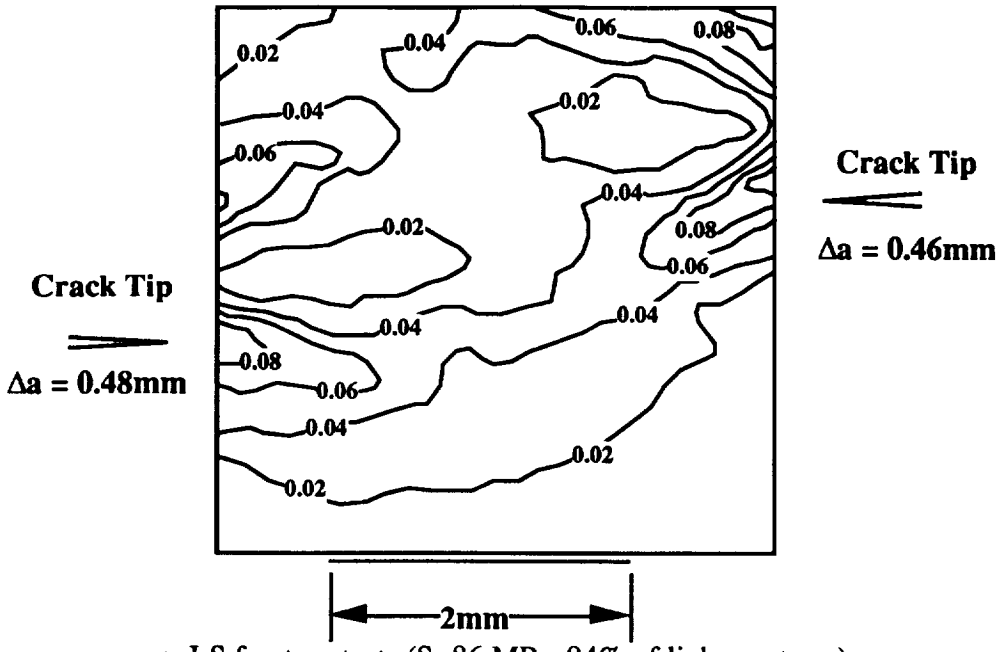

a. LS fracture tests (S=86 MPa, 94% of link-up stress)

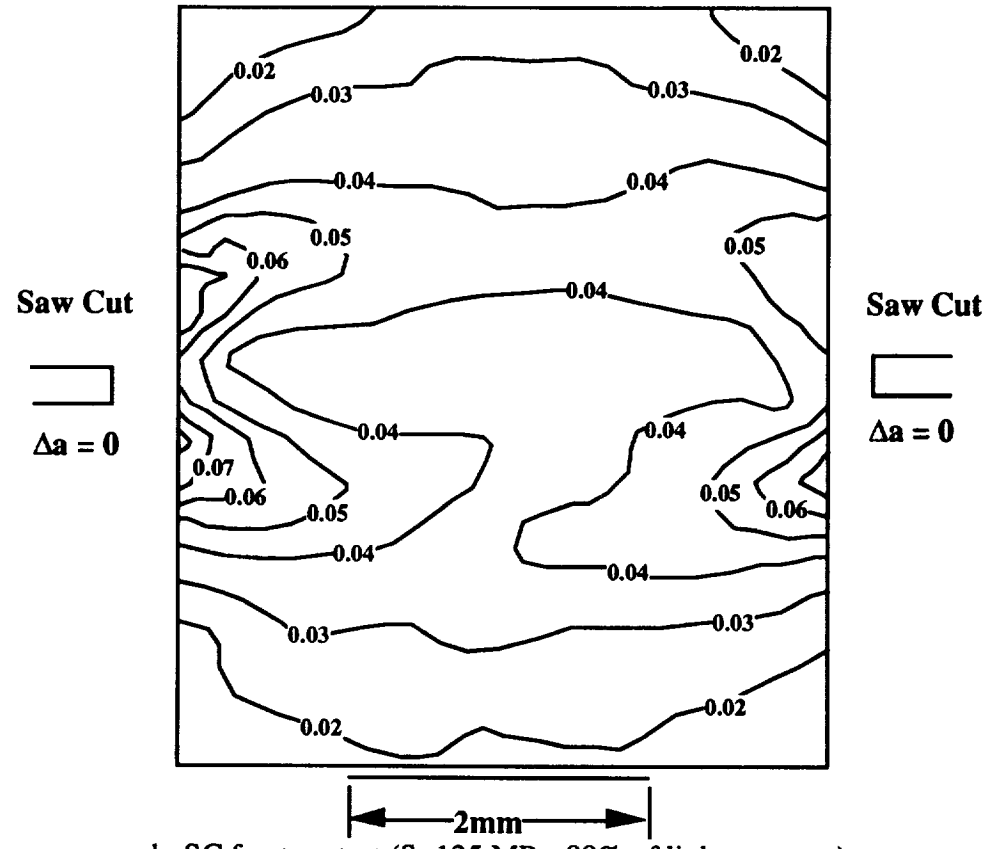

b. SC fracture test (S=125 MPa, 99% of link-up stress)

Figure 11 ε_{yy} strain fields for the ligament between two cracks 5.1mm apart.

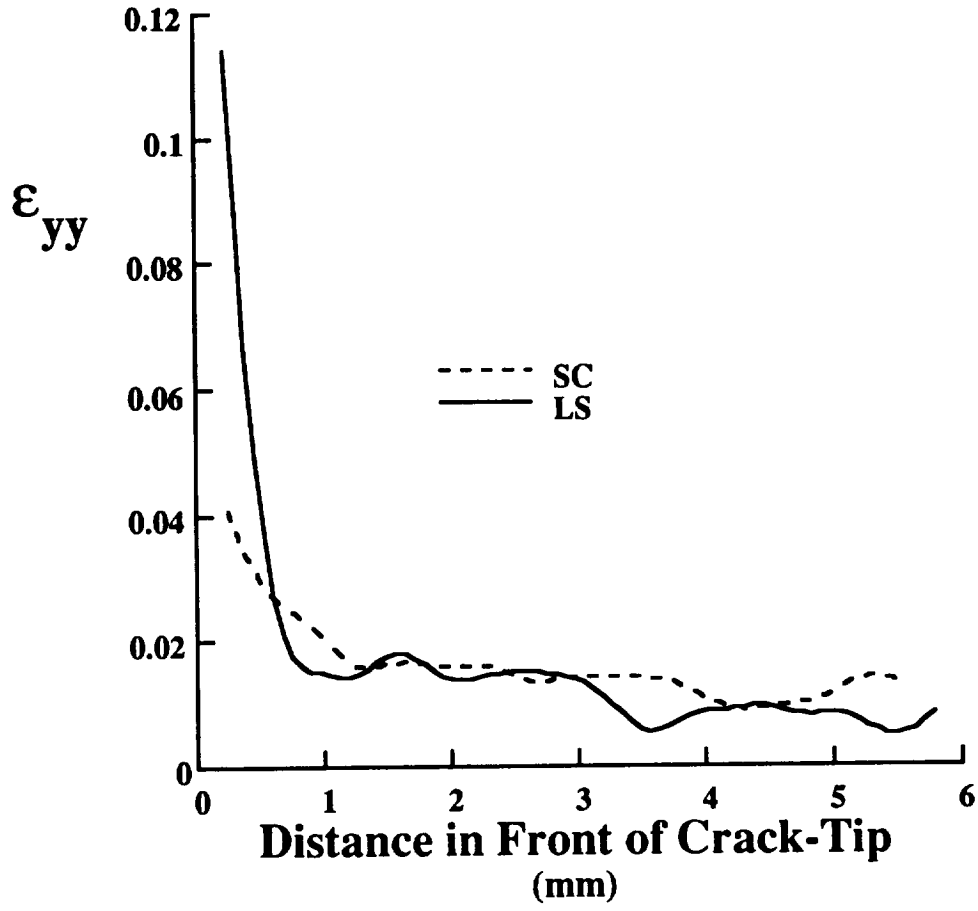

Figure 12 The ε_{yy} strain as a function of distance from crack tip, S=230 MPa.

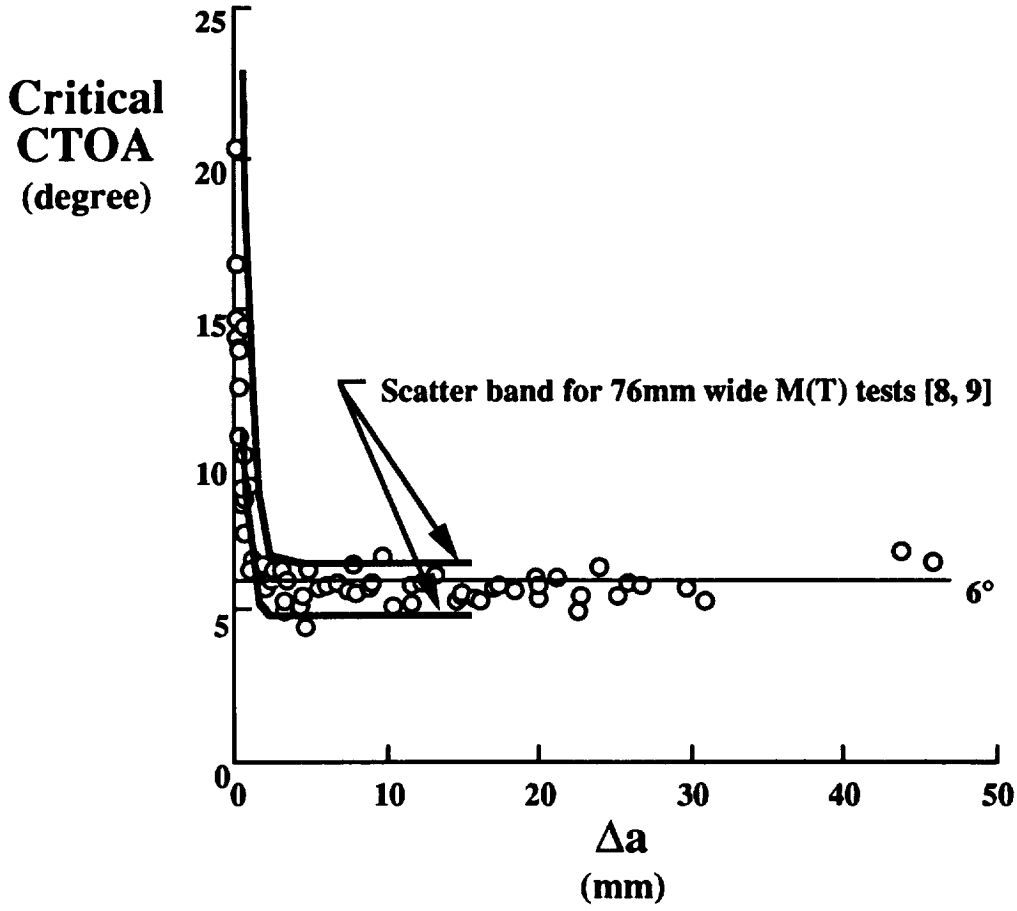

Figure 13 Critical crack-tip opening angles measured for the 305mm wide LS tests and the scatter band for the 76mm wide LS M(T) tests [8,9].

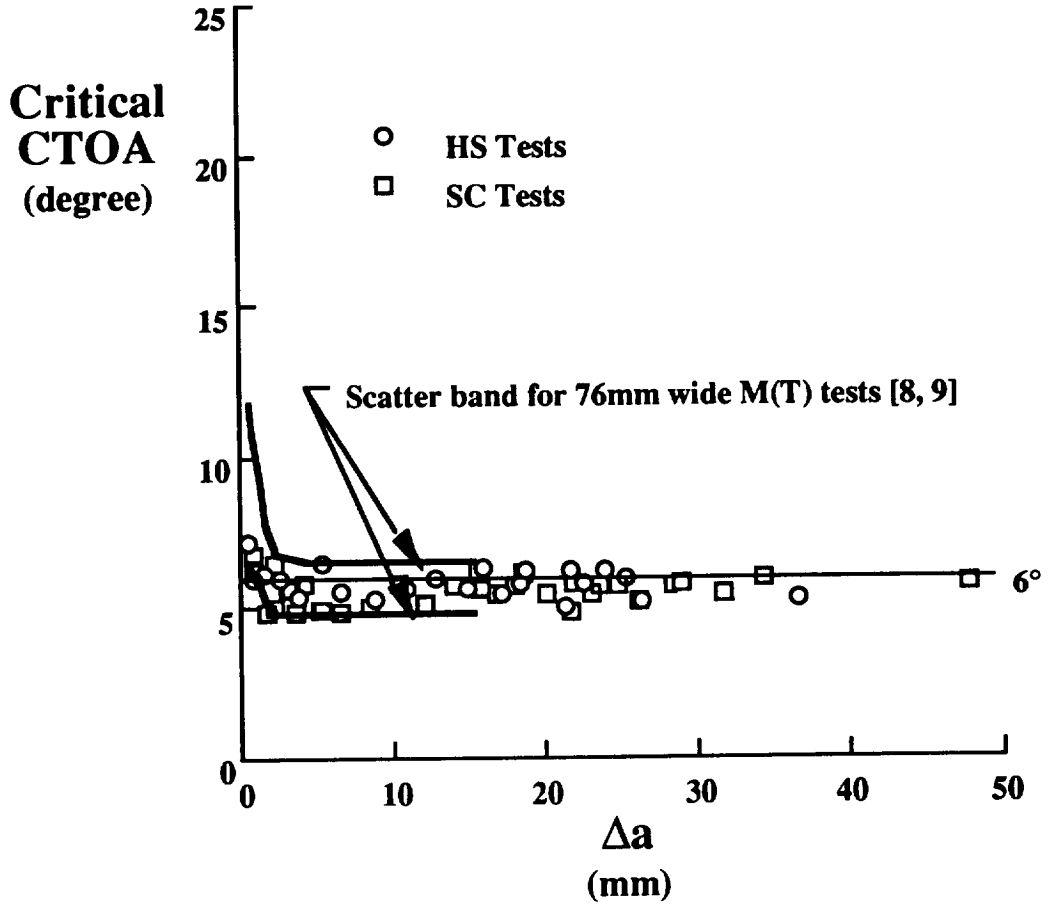

Figure 14 Critical crack-tip opening angles measured for the 305mm wide HS and SC tests and the scatter band for the 76mm wide M(T) HS tests [8,9].

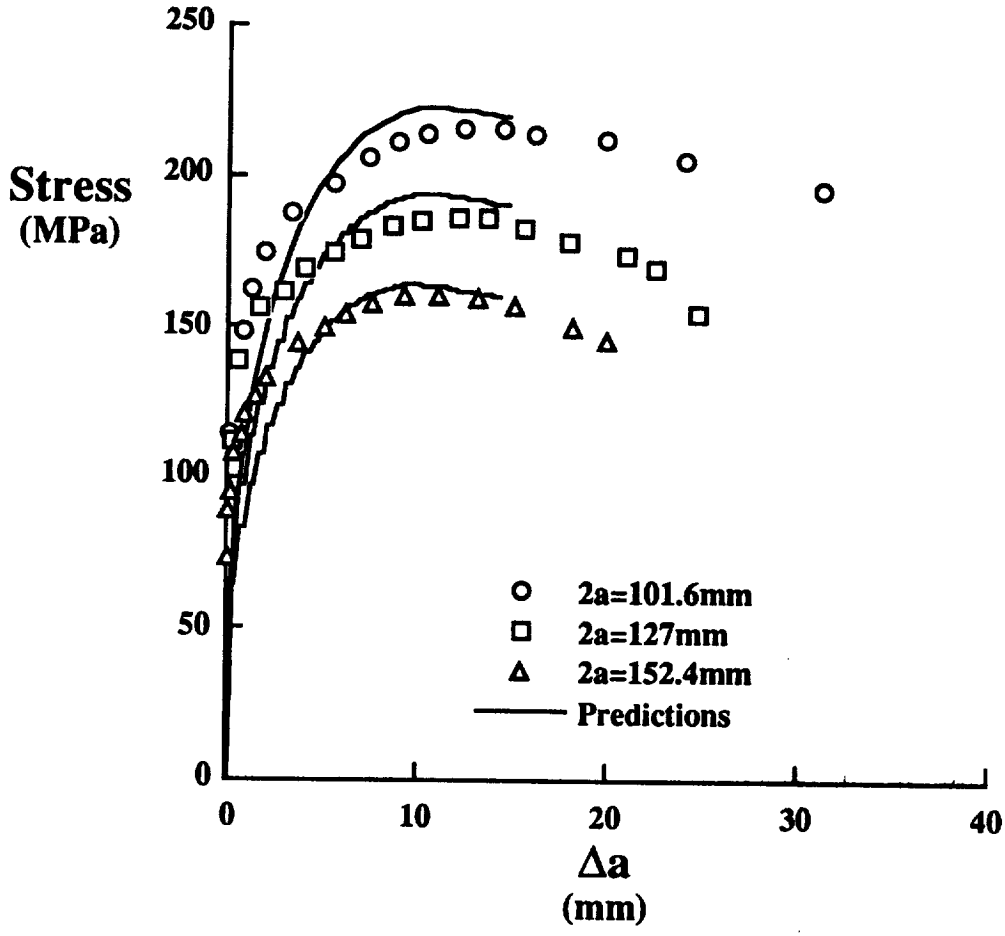

Figure 15 Stress against crack extension for the 305mm wide single crack LS tests.

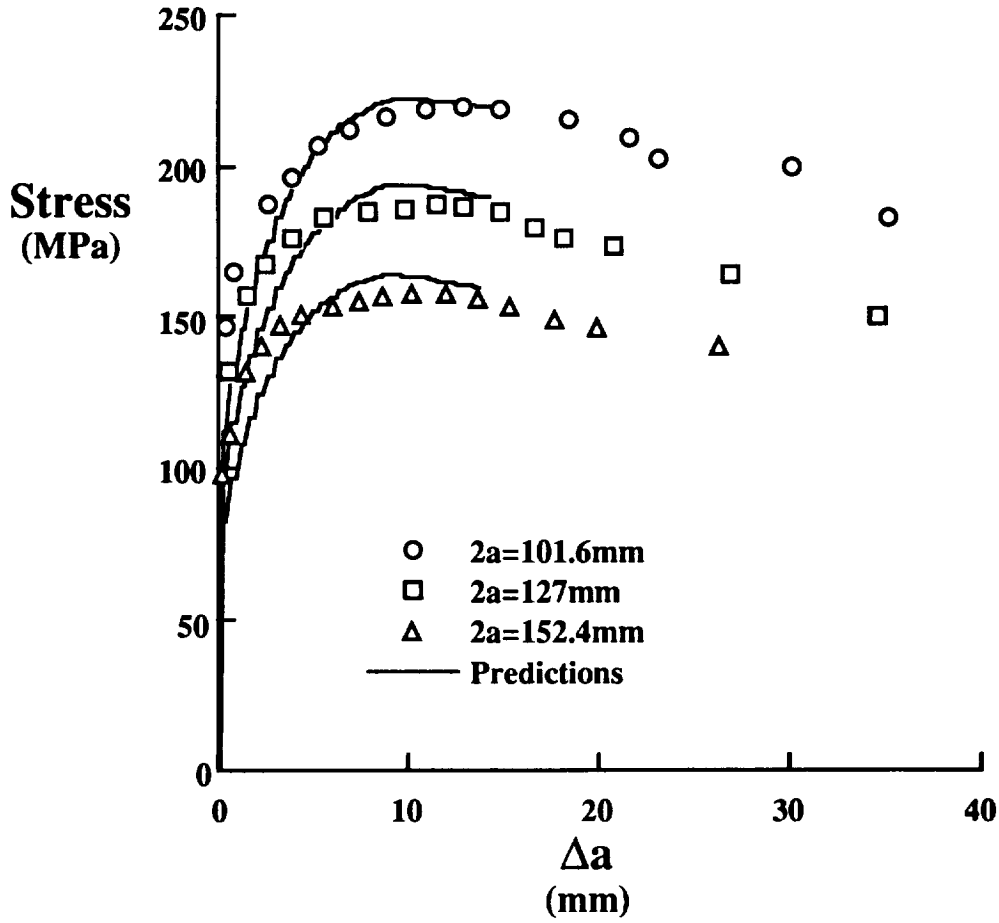

Figure 16 Stress against crack extension for the 305mm wide single crack HS tests.

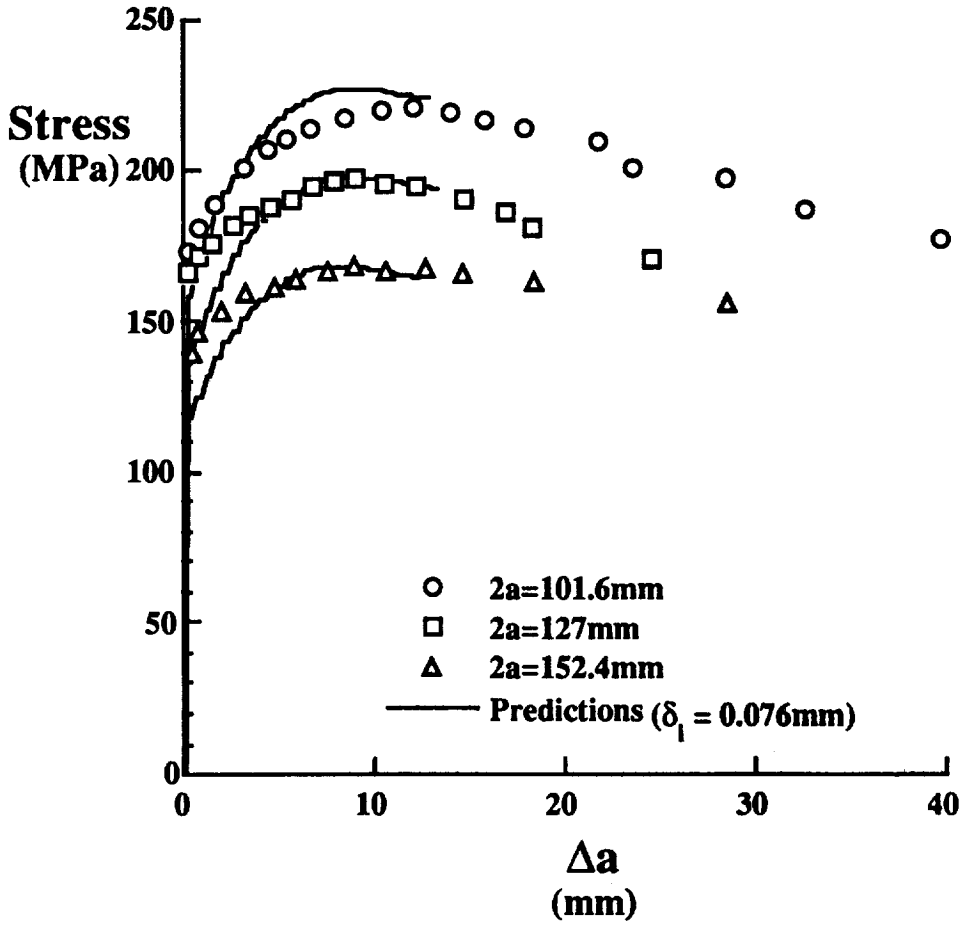

Figure 17 Stress against crack extension for the 305mm wide single crack SC tests.

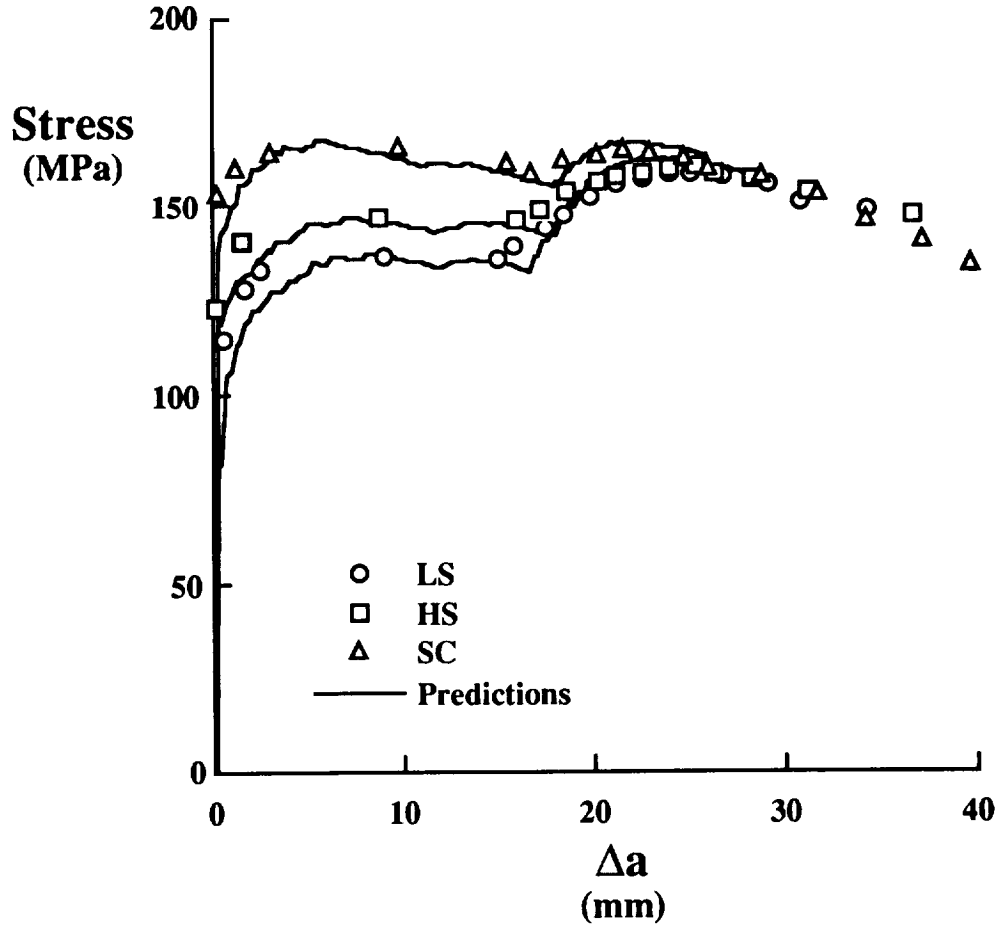

Figure 18 Stress against crack extension for three 305mm wide 3-crack (small ligaments between cracks) fracture tests.

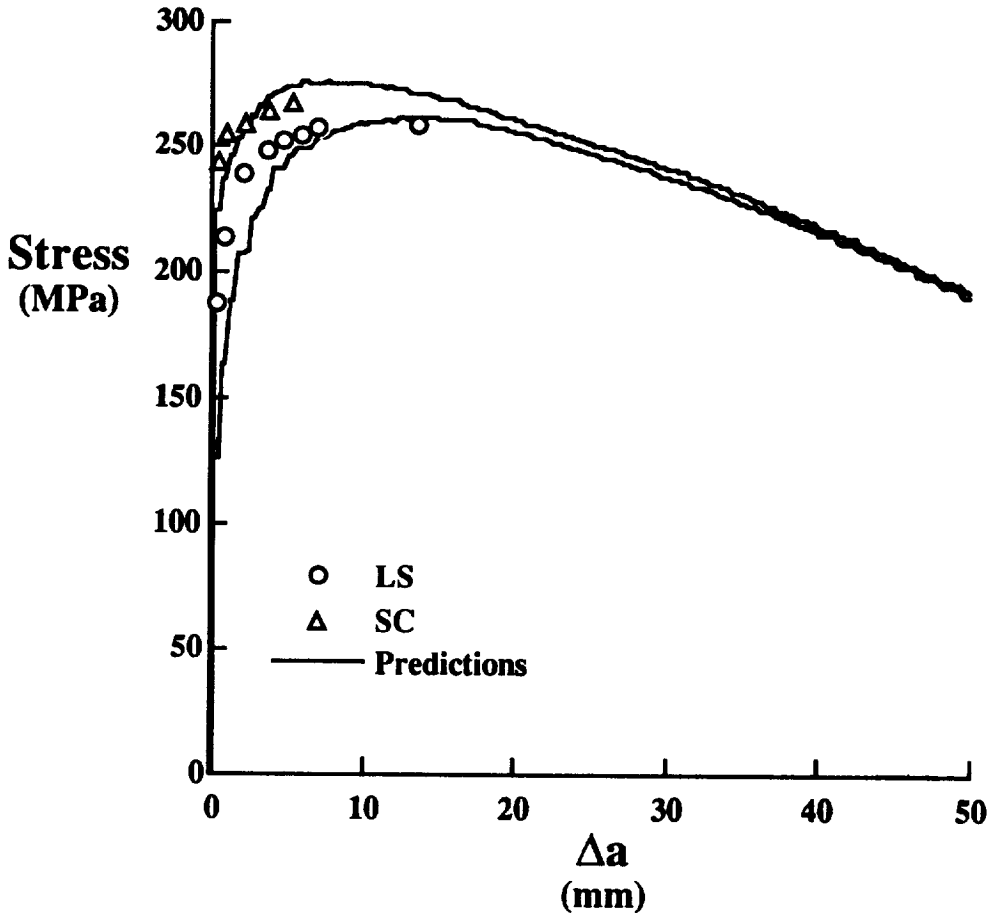

Figure 19 Stress against crack extension for two 305mm wide 3-crack (large ligaments between cracks) fracture tests.

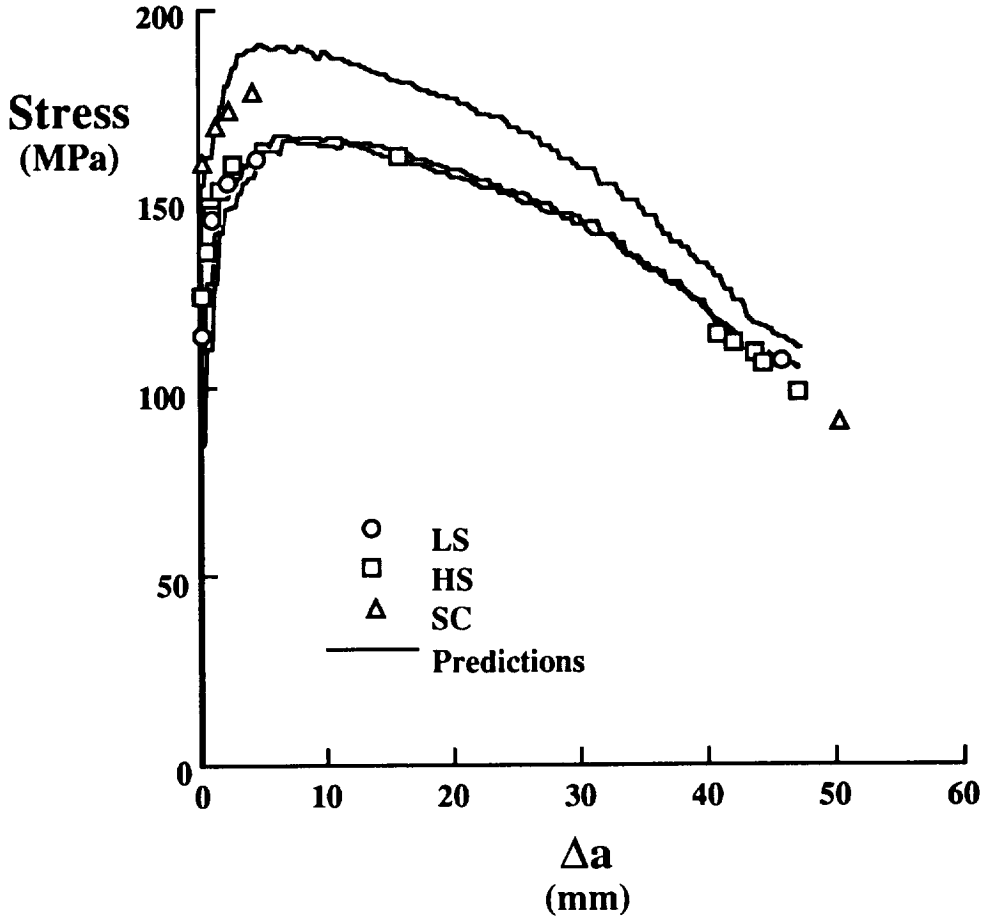

Figure 20 Stress against crack extension for three 305mm wide 5-crack fracture tests.

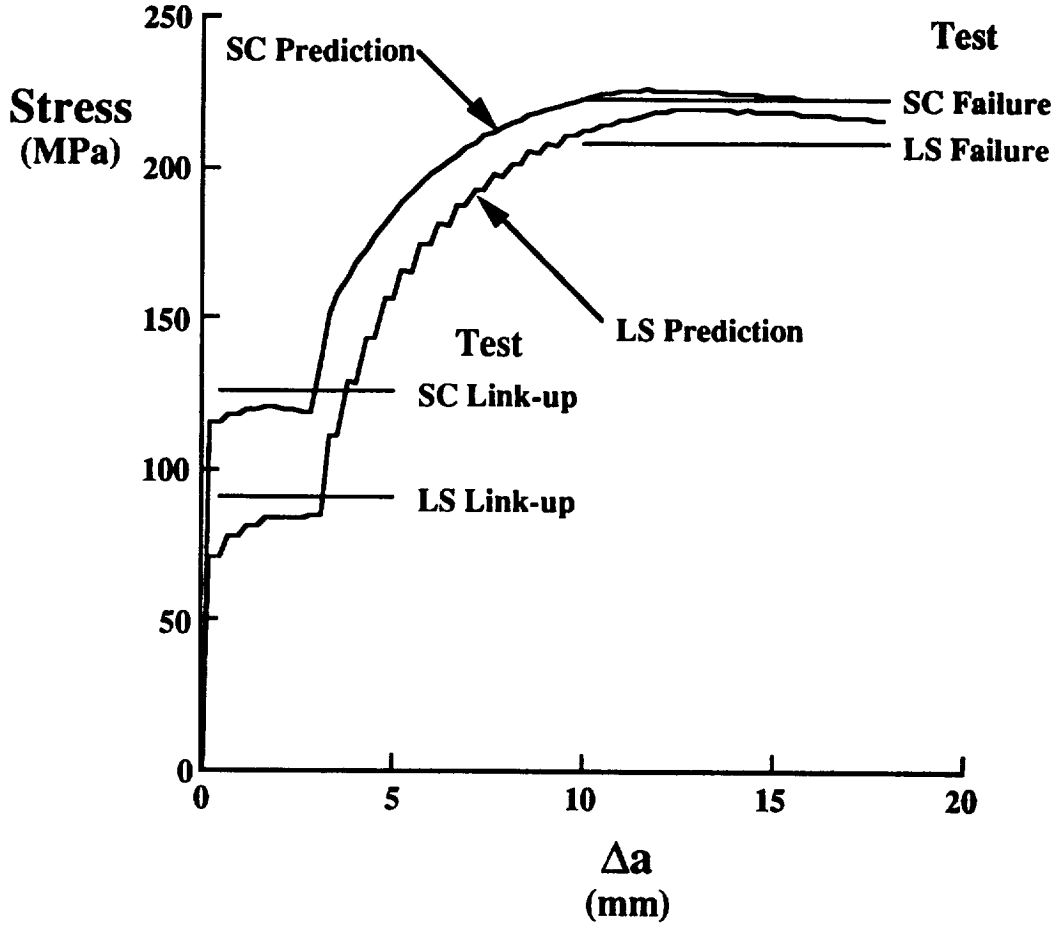

Figure 21 Stress against crack extension for two 305mm wide 2-crack (5mm ligament between cracks) fracture tests.

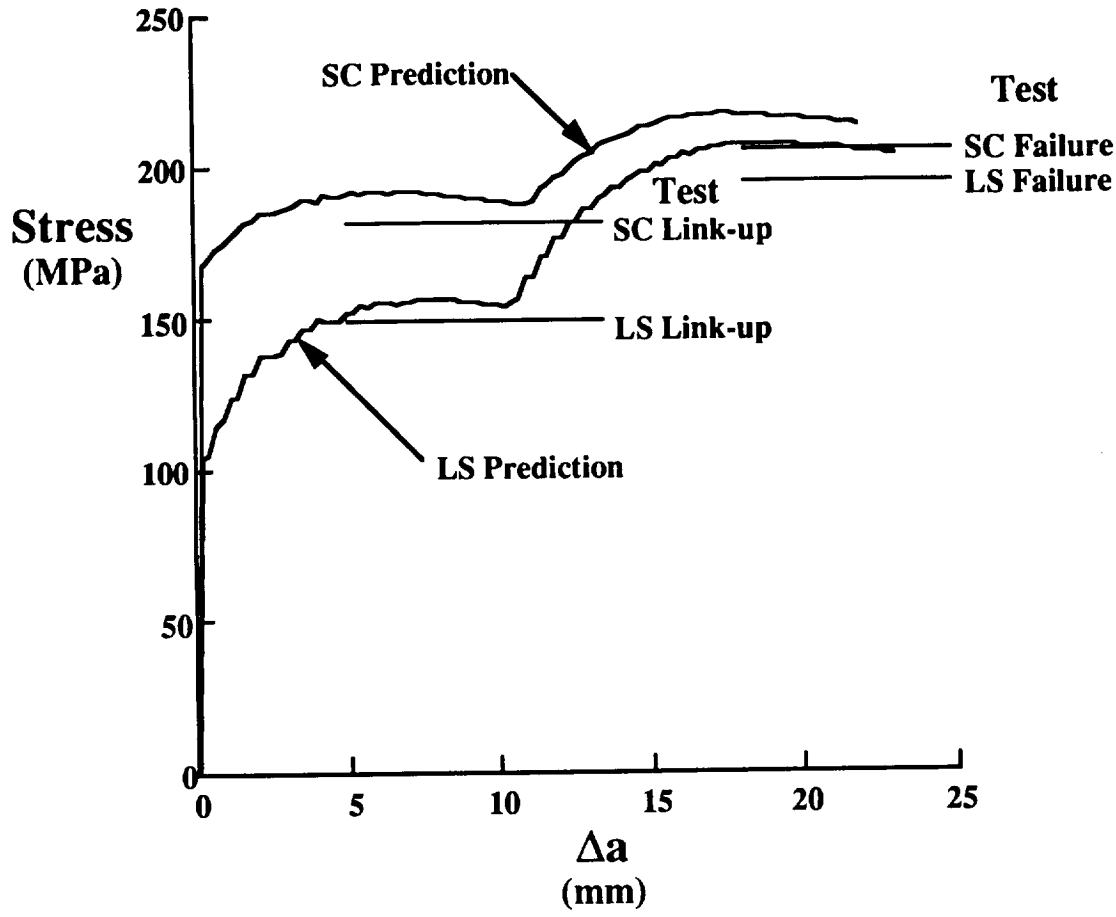

Figure 22 Stress against crack extension for two 305mm wide 2-crack (15mm ligament between cracks) fracture tests.

REPORT DOCUMENTATION PAGE

Form Approved
OMB No. 0704-0188

1. AGENCY USE ONLY (*Leave blank*)	2. REPORT DATE	3. REPORT TYPE AND DATES COVERED
	July 1994	Technical Memorandum

4. TITLE AND SUBTITLE
Stable Tearing Behavior of a Thin-Sheet Material with Multiple Cracks

5. FUNDING NUMBERS
WU 538-02-10-01

6. AUTHOR(S)
D. S. Dawicke, J. C. Newman, Jr., M. A. Sutton, and B. E. Amstutz

7. PERFORMING ORGANIZATION NAME(S) AND ADDRESS(ES)
NASA Langley Reserch Center
Hampton, VA 23681-0001

8. PERFORMING ORGANIZATION REPORT NUMBER

9. SPONSORING / MONITORING AGENCY NAME(S) AND ADDRESS(ES)
National Aeronautics and Space Administration
Washington, DC 20546-0001

10. SPONSORING / MONITORING AGENCY REPORT NUMBER
NASA TM-109131

11. SUPPLEMENTARY NOTES
D. S. Dawicke: Analytical Services and Materials, Inc., Hampton, VA; Newman, Jr.,: Langley Research Center, Hampton, VA; M. A. Sutton and B. E. Amstutuz: University of South Carolina, Columbia, SC.

12a. DISTRIBUTION / AVAILABILITY STATEMENT
Unclassified-Unlimited

Subject Category 26

12b. DISTRIBUTION CODE

13. ABSTRACT (*Maximum 200 words*)

Fracture tests were conducted on 2.3mm thick, 305mm wide sheets of 2024-T3 aluminum alloy with from one to five collinear cracks. The cracks were introduced (crack history) into the specimens by three methods: saw cutting, fatigue precracking at a low stress range, and fatigue precracking at a high stress range. For the single crack tests, the initial crack history influenced the stress required for the onset of stable crack growth and the first 10mm of crack growth. The effect on failure stress was about 4% or less. For the multiple crack tests, the initial crack history was shown to cause differences of more than 20% in the link-up stress and 13% in failure stress. An elastic-plastic finite element analysis employing the CTOA fracture criterion was used to predict the fracture behavior of the single and multiple crack tests. The numerical predictions were within 7% of the observed link-up and failure stress in all the tests.

14. SUBJECT TERMS
Fracture; Crack-top opening angle; Experiments; Elastic-plastic finite elements; Predictions

15. NUMBER OF PAGES
40

16. PRICE CODE
A03

17. SECURITY CLASSIFICATION OF REPORT	18. SECURITY CLASSIFICATION OF THIS PAGE	19. SECURITY CLASSIFICATION OF ABSTRACT	20. LIMITATION OF ABSTRACT
Unclassified	Unclassified		